Facultad de Ciencias

Primordial black holes as dark matter candidates: analysis of observational constraints with LIGO/Virgo

(Agujeros negros primordiales como candidatos de materia oscura: análisis de las cotas observacionales con LIGO/Virgo)

Trabajo de Fin de Grado
para acceder al

Grado en Física

Autor: Abram Pérez Herrero

Director: Diego Herranz Muñoz

Codirector: Bradley James Kavanagh

Junio - 2021

Agradecimientos

En primer lugar me gustaría agradecer a mi familia.
A mi madre,
por todo su apoyo y cariño durante tantos años.
A mi padre,
por su fuerza y su curiosidad,
ya que toda esta aventura empezó por ti.
A Adrián,
por ir siempre delante abriendo camino
y por todas esas risas en los tres años de convivencia juntos.
A Ángela,
por acompañarme en mis locuras y hacerme reír siempre.
A Aitor,
por su compañía y por divertirme tanto a su lado.
A Aroa,
por su entusiasmo contagioso y su energía.
También, me gustaría agradecer a mis abuelas,
por sus ánimos y sus abrazos.
Al resto de la familia y amigos.
A María,
por hacer que estos tres años se me hayan pasado volando
y por ayudarme tanto con este trabajo.
A su familia,
por acogerme tantos fines de semana estos últimos años.
A Diego,
por ayudarme a elaborar este trabajo.
Finally, to Bradley for answering all my doubts, which were not few,
and for helping me to develop all this work.

Abstract

The cosmological concordance model considers that approximately about twenty per cent of the energy/material composition of the Universe is constituted by some non-baryonic, non-interacting matter (except through gravitation and, perhaps, weak interaction) that is known as dark matter. Although there is much indirect observational evidence for the existence of dark matter, we have so far been unable to obtain any direct observation of it, and there is not even a consensus on which particles (outside the standard model) might constitute it. Among the many candidates that have been proposed to explain dark matter, one of the most interesting for modern cosmology is primordial black holes. Such primordial black holes could have been formed spontaneously from extreme local overdensities as a result of density fluctuations that emerged during the first moments after the Big Bang.

In this work, we will review the theoretical background behind this idea, starting from simple models and then relaxing some of the assumptions of these models to consider more realistic scenarios. Subsequently, we will use the most recent gravitational wave observations from the public data of the LIGO and Virgo experiments to update, if possible, the current estimations of the contribution of primordial black holes to the total dark matter budget $f_{\rm PBH}$, as a function of its mass in the range $[10^{-1},\, 10^{3}]$ $\mathrm{M}_{\odot}$ that form short-period binary systems.

We have estimated that the maximum fraction of dark matter that primordial black holes constitute for a simple model is of the order of $f_{\rm PBH} \approx 10^{-4}$ in the mass range $[10^{0},\, 10^{2}]$ $\mathrm{M}_{\odot}$, becoming less restrictive for the rest of the mass range. When we have considered more realistic cases these constraints become weaker, obtaining a value of the order of $f_{\rm PBH} \approx 10^{-3}$ in the mass range $[10^{0},\, 10^{2}]$ $\mathrm{M}_{\odot}$.

Keywords: Primordial black holes, Dark matter, Gravitational waves, LIGO, Virgo, PBH constraints.

Resumen

El modelo de concordancia cosmológico considera que aproximadamente un veinte por ciento del contenido energético/material del Universo está constituido por algún tipo de materia no bariónica y no interactuante (salvo a través de la gravitación y, tal vez, de la interacción débil) que recibe el nombre de materia oscura. Aunque existen numerosas evidencias observacionales indirectas de la existencia de la materia oscura, por el momento no hemos podido obtener ninguna observación directa de la misma y ni siquiera existe consenso acerca de qué tipo de partículas (fuera del modelo estándar) pueden constituirla. De entre los muy variados candidatos que se han propuesto para explicar la materia oscura, uno de los más interesantes para la cosmología moderna son los agujeros negros primordiales. Dichos agujeros negros primordiales podrían haberse formado espontáneamente a partir de sobredensidades locales extremas fruto de las fluctuaciones de densidad que emergieron durante los primeros instantes tras el Big Bang.

En este trabajo revisaremos los fundamentos teóricos que subyacen tras esta idea, partiendo de modelos sencillos y posteriormente relajando algunas de las suposiciones de dichos modelos para considerar situaciones más realistas. Posteriormente, haremos uso de las más recientes observaciones de ondas gravitacionales a través de los datos públicos de los experimentos LIGO y Virgo para actualizar, si es posible, las cotas actualmente existentes a la posible contribución de agujeros negros primordiales al balance total de materia oscura f_{PBH}, en un rango de masas de agujeros negros primordiales $[10^{-1},\ 10^{3}]$ $\mathrm{M}_{\odot}$ que forman sistemas binarios de periodo corto.

Se ha estimado que la fracción máxima de materia oscura que constituyen los agujeros negros primordiales asumiendo un modelo sencillo, es del orden de $f_{\mathrm{PBH}} \approx 10^{-4}$ en un rango de masas $[10^{0},\ 10^{2}]$ $\mathrm{M}_{\odot}$, volviéndose menos restrictivas para el resto del rango de masas. Cuando se consideran casos más realistas esta cota se vuelve menos restrictiva, obteniéndose un valor de dicha fracción del orden de $f_{\mathrm{PBH}} \approx 10^{-3}$ en un rango de masas $[10^{0},\ 10^{2}]$ $\mathrm{M}_{\odot}$.

Palabras clave: Agujeros negros primordiales, Materia oscura, Ondas gravitacionales, LIGO, Virgo.

Index

Chapter 1

Introduction

Physics, by definition, is the science that deals with energy, matter and the interactions between them. However, despite great progress has been made by the physicists in understanding the matter and energy that compound our Universe, we still know too little about the 95% of them.[1] This large part that we still do not understand is composed of dark energy and dark matter (DM), which constitute the 68% and 27% of the Universe respectively. In this work, we deal with the search for dark matter since it is a field that has been rapidly growing in recent years.

Dark matter is believed to be a kind of matter that interacts mainly via gravitation force. In fact, its discovery by Fritz Zwicky occurred by comparing the mass of galaxy clusters to their luminosity, observing that there exist some invisible matter that does not contribute to its luminosity. Currently, we know more properties about the dark matter thanks to the study of its dynamics in galaxies and galaxy clusters and of the role it plays in the formation and evolution of the large scale of the Universe. We know, for example, that dark matter particles are cold, i.e. they do not move at relativistic speeds, because otherwise dark matter would not remain bound in gravitational wells where galaxy clusters could be formed. We also know that dark matter particles must be non-baryonic, because otherwise they would have played a dramatic effect in the nuclear reactions that took place during the Big Bang Nucleosynthesis (BBN) and the Universe's chemical composition would be very different to what we observe today. Additional evidence of the non-baryonic nature of dark matter come from the study of the Cosmic Microwave Background (CMB) temperature anisotropies.

During the last few decades, many dark matter candidates have been proposed, from more or less exotic kinds of particles, like axions, to larger compact astrophysical objects. A dark matter candidate, which is being a source of potential interest, are primordial black holes (PBH). The PBHs are hypothetical black holes that were formed in the early Universe by the collapse of large density perturbations. This candidate of cold dark matter is non-baryonic since it was formed before the BBN and it only interacts via gravitational force. Moreover, their formation mechanism allows a very large range of possible masses that could explain some cosmological features like the matter-antimatter asymmetry [2] or the galaxies formation [3].

The existence of primordial black holes causes observable effects on different features of the Universe. For that reason, the study of PBHs is based on using these features to place constraints in the fraction of dark matter that they constitute. It is given by $f_{\rm PBH} = \Omega_{\rm PBH}/\Omega_{\rm DM}$, where $\Omega_{\rm PBH}$ is the density parameter for primordial black hole density and $\Omega_{\rm DM}$ is the density parameter for dark matter density. We will see some of these constraints in Figure 1.1, where the shaded regions show the $f_{\rm PBH}$ values that cannot be taken because they are greater than their maximum value. The effects used to obtain these constraints are:

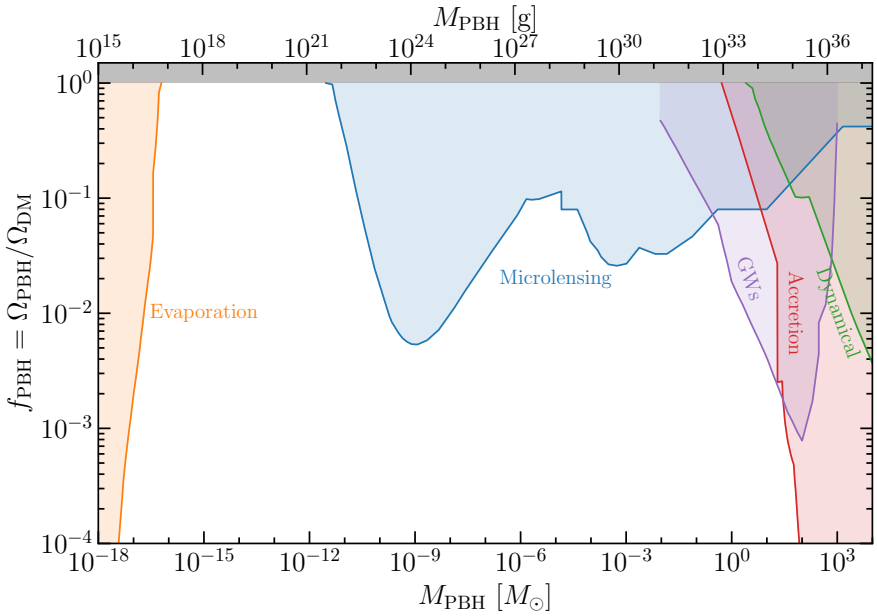

Figure 1.1: Main constraints on the fraction of dark matter $f_{\rm PBH}$ in the form of PBHs with mass $M_{\rm PBH}$. In this case, it has considered monochromatic mass function and initial uniform distribution of PBHs.[4]. *Shaded regions:* the $f_{\rm PBH}$ values that cannot be taken because they are greater than their maximum value.

- **Evaporation.** "Black holes evaporation" is based on the black hole mass reduction due to the emission of Hawking radiation. This hypothetical radiation increases when the isolated black hole has a lower mass, reducing its half-life. Therefore, it is possible to establish lower constraints considering that the primordial black holes that constitute dark matter have to be stable up to the present day. These lower constraints are given by $M_* \approx 10^{-18}\,{\rm M}_\odot$, i.e. the primordial black hole whose mass is less than M_* have already completed their evaporation, and hence do not constitute dark matter at present. Furthermore, a little more massive PBH ($M_* < M_{\rm PBH} < 10^{-16}{\rm M}_\odot$) should currently be evaporating, producing in the process a γ-ray background [5] or energetic particles like neutrinos [6] which are detectable. These observable effects could be used to set constraints to their abundance.

- **Microlensing.** The microlensing effect occurs when a massive compact object is located along the line of sight of a light source and the observer, causing distortion or amplification of that light. The PBHs with masses in the range of $10^{-11}\,{\rm M}_\odot <$

$M_{PBH} < 10^3\ M_\odot$ could produce this effect in a measurable form for us. There exist different microlensing experiments depending on the type of light source the commons are the study of stars [7], quasars [8] and supernovae [9]. As black hole evaporation, the measurements based on this effect provide constraints on the dark matter fraction.

- **Accretion** As compact objects, primordial black holes attract gas and dust around them, giving rise to an accretion disc. In the nearest part of the accretion disk, the energy density is huge due to the high rotational speed and friction. This energy density is high enough to emit X-rays [10] and naturally radio waves [11], which are detectable from the Earth. These detections result in an upper constraint for the PBH with a mass greater than one solar mass. It is also possible to derive the constraints from the distortion of the cosmic microwave background (CMB) caused by the density perturbation of large PBHs masses. [12]

- **Dynamical.** The primordial black holes exert an interaction with their environments. Consequently, if the PBHs exist, it could produce effects like the collisions with stars, changes in wide binaries spatial distribution or energetic interactions with neutron stars [13] and white dwarfs [14]. All these effects produce constraints on the abundance of massive PBHs since we could indirectly detect them.

- **Gravitational waves.** There exists the possibility that the primordial black holes formed a binary system in the early Universe. These binary systems produce gravitational waves (GW), as they are accelerated objects so massive that they disturb space-time, propagating through space at the speed of light. The emission of these GW causes the loss of energy from the system, which could cause them to merge. That merge generates waves so intense that they are detectable with ground-based detectors such as LIGO/Virgo. These detections allow us to establish the possible merger rate of binaries that are merging at present. As both the number of binaries and the number of binaries that eventually merge will depend on the initial conditions of the PBHs, we can obtain information from them. Among these initial conditions, we could obtain the maximum abundance of PBHs. [15] Also, it is possible to establish the abundance's constraints by measuring a stochastic background of gravitational waves since many of the binaries could have merged given such a residual background.[16]

The last constraint is becoming popular since binary black holes are now being detected by experiments such as LIGO and Virgo. The binary black holes detected are of unknown origin so they could be primordial black holes. These detections have raised curiosity as they could be a direct detection of dark matter.

In this work, we will focus on the study of GW abundance constraints given by the merge of primordial black holes binaries at present. For this purpose, we will perform a theoretical calculation of the merger rate that will be compared with the most recent data provided by LIGO/Virgo. In this way, we will not only analyse the constraints but will also allow us to update them. This estimation requires knowledge of the initial properties, which are currently unknown, and the different effects during their evolution. The main

initial conditions that determine each model are the initial spatial distribution and the initial mass function.

As the process of formation of these primordial black holes is not completely defined, there is a possibility that they could have an initial uniform spatial distribution (IUSD) or initial clustered spatial distribution (ICSD). Although it is thought that the most probable situation is that the distribution is uniform, the other possibility has to be considered. On the other hand, the mass function, which corresponds to the probability that the PBH initially had a certain mass, can be classified into extended mass functions (EMF) and monochromatic mass function (MMF). The extended mass function considers that probability of the PBHs have a range of mass, and in the monochromatic mass function, it is considered that all black holes have the same mass. In Figure 1.2, it is shown the diagram of the different models that we will consider. All these models have been developed over the years and improved as more information is found both from LIGO/Virgo detections and from the possible formation scenario. Also, the interaction of the black holes with their initial environment conditions (IEC) is considered in the models.

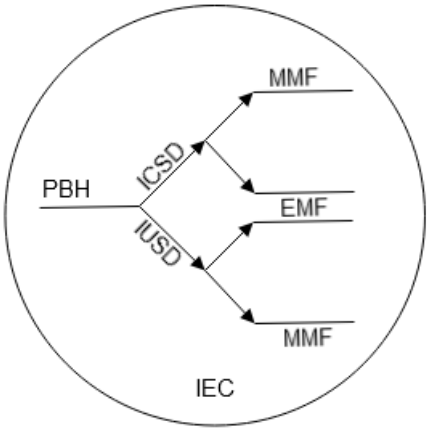

Figure 1.2: Schematic representation of different models that we will consider to estimate the merger rate. We denoted as ICSD the initial clustered spatial distribution, as IUSD the initial uniform spatial distribution, as MMF the monochromatic mass function, as EMF the extended mass function and IEC, as the initial environmental conditions.

Whether they constitute all dark matter or only a fraction, primordial black holes could explain many cosmological features, [17] as well as provide a better understanding of our Universe. That is the reason why PBH have become a hot topic in the literature, particularly since LIGO/Virgo started reporting GW merger events in 2015.

1.1. Objectives and structure of the work

The structure of this work will be divided into three chapters.

- **Chapter 2**. It aims to provide the reader with a background on primordial black holes. It will introduce concepts such as their formation, their evolution when they

form binary systems, and how we can detect them. In addition, some concepts will be introduced in detail as they will be used in the following chapters, so we recommend reading them before the subsequent chapters. Some knowledge of General Relativity is required.

- **Chapter 3**. This is the main chapter of the work and its objective is the theoretical development of the merger rate of primordial black holes. We will first seek to obtain its expression for the simplest case, where all black holes are assumed to have the same mass. Then, we will generalise this development to more realistic or different cases, such as the case of a spatial clustering distribution. Additionally, we will observe the behaviour of the total merger rate in each case. Some of the developments that help to follow the chapter have been added in **Appendix A**.

- **Chapter 4** Finally, we will obtain the PBH abundance constraints comparing the previously developed theoretical models with the most recent experimental analysis published from LIGO/Virgo measurements. In some cases, we will use the most recent data getting to update it. These constraints will allow us to compare different models and a general idea of the fraction of dark matter that these primordial black holes constitutes in the mass range $[10^{-1},\ 10^{3}]\ \mathrm{M}_{\odot}$ will be also given at the end of the chapter. In this way, we can characterise and learn more about this dark matter candidate.

It is noteworthy that a set of numerical calculations will also be done both to obtain the plots shown throughout the work and to provide all PBH constraints. These codes can be obtained from `https://github.com/AbramPerezHerrero/MergeRatePBH.git`.

It will be considered throughout the work that $c = G = 1$.

Chapter 2

Evolution of primordial black holes

In this chapter, we will first discuss briefly their possible origin focusing on the simplest case that is the collapse of large density fluctuation, in 2.1. We will then deal with the case where primordial black holes form binary systems and their evolution. As will be seen in 2.2, they are characterised by the emission of gravitational waves, which will gradually reduce the energy of the system. Finally, in section 2.3, the merger of such binary systems will be discussed, in particular the observations that these events produce.

2.1. Primordial black holes formation

There exist many theories about the formation of primordial black holes since the conditions in the early Universe are unknown. Some of the more exotic ones are collapse of cosmic loops, collapse of domain walls and bubble collision.[5] However, one of the well-studied scenarios involves the collapse of large density perturbations in the early Universe. Whatever the origin of these fluctuations is, they could cause overdensities capable of opposing the expansion of the Universe and collapse, forming a black hole. In this section, we will briefly explain this formation scenario, which will serve as a background to understand the reason this work deals with different models. In-depth theoretical analysis is out of the scope.

2.1.1. Large density fluctuations

The first physicists that deal with primordial black holes were Stephen Hawking and Bernard Carr.[18]. They started from the idea that the early Universe had to be inhomogeneous and highly dense to form galaxies or other large-scale structures. In this inhomogeneous early Universe, ordinary density perturbations could exist with a density large enough for the gravitational force to be stronger than the radiation pressure and the expansion of the Universe. This process is similar to type II supernovae, where the compression of matter can produce a compact object such as a black hole. Therefore, if the density contrast $\delta \equiv (\rho - \bar{\rho})/\bar{\rho}$, where ρ is the density and $\bar{\rho}$ is the background density, exceeds a critical density threshold δ_c, which considers the opposite effects of collapse, there exists the possibility of forming a primordial black hole. We will see this mechanism in Figure 2.1.

Hawking and Carr considered that the Schwarzschild radius of primordial black holes had to be similar to the value of the horizon radius at the time of formation. Their explanation for this was that a smaller Schwarzschild radius would imply that collapse had already occurred earlier, and a larger radius would imply that collapse had not yet occurred. Taking this equality as a starting point, the mass of the primordial black hole as a function of time can be expressed as

$$M_{pbh} \sim M_H = \frac{4\pi}{3}\bar{\rho}\left(\frac{1}{H}\right)^3 \sim 10^{15}\,\mathrm{g}\left(\frac{\mathrm{t}}{10^{-23}\,\mathrm{s}}\right)\,, \tag{2.1}$$

where M_H is the horizon mass, which is the mass given by the volume of the Hubble horizon during the radiation era. This mechanism allows, as mentioned above, the PBH mass range to be so wide.

Therefore, in the simplest scenario, following the equation (2.1), if all primordial black holes were created at a specific time, they could have the same mass, i.e. a monochromatic mass function. However, there exists some deviation of this simple scenario. One of these deviations is the critical collapse in which the PBH mass still depends on the horizon mass. Nevertheless, there is a relationship between the mass of primordial black holes and the amplitude of the density perturbation. This theory of critical collapse was developed in the 1990s since critical collapse could occur when the density perturbations reach the density threshold.[4] This relationship is given by

$$M_{\mathrm{PBH}} = \kappa M_H(\delta - \delta_c)^\gamma\,, \tag{2.2}$$

where γ and κ are parameters that depend on the shape of the density perturbations and the equation of state of the expanding Universe[19].

An important fact to note is the spin of primordial black holes. The spin of the astrophysical [1] black holes is large since, by conservation of angular momentum, when the black hole is formed by the rotating gas, it has to spin very quickly. However, this does not happen with primordial black holes in this formation scenario since if we consider the isotropic principle, the total rotation of the density perturbation is null. Therefore, We expect that the PBHs have not spin or have a slight spin provided by the influence of other compact objects (of an order of 0.01). This effective spin is measurable by merging binary black holes in LIGO and Virgo. [20]

This formation mechanism does not provide us with a concrete initial spatial distribution of PBHs, as it depends on the type of primordial perturbations that were present in the early Universe. These perturbations are usually modelled as a Gaussian random field whose fluctuations have physical scales that are described by a given power spectrum. Structures (including PBHs) can collapse around the positions of the local maxima of the fluctuation field if the density exceeds a certain critical threshold. The positions of these maxima can be uncorrelated among each other, or they can be clustered across scales defined by the power spectrum (or, equivalently, the two-point correlation function). Figure

[1] We denote as astrophysical to the black holes which origin is stellar.

2.1 shows both scenarios: PBH formation with (right panel) and without clustering (left panel).

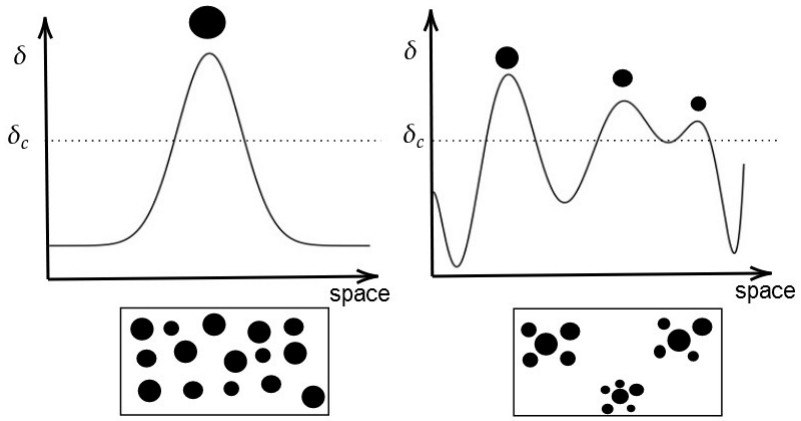

Figure 2.1: Representation of two different density perturbations examples in the function of space. *Left:* Gaussian perturbation in a certain volume without spatial correlation with the others density perturbations which implies initial uniform spatial distribution, illustrated in the panel below. *Right:* three Gaussian perturbations in a certain volume with spatial correlation, which implies clustered initial distribution, illustrated in the panel below.

Primordial black holes must have been formed before the Big Bang Nucleosynthesis (BNN) because otherwise, as we have discussed above, they would have played a dramatic effect in the nuclear reactions that took place during the Big Bang Nucleosynthesis and the Universe's chemical composition would be very different to what we observe today. For that reason, if we consider the standard model of Big Bang cosmology, the radiation domination era is the only stage that the PBHs could have been formed. Although there are some exotic cosmological models where a matter domination era occurred before BBN, they still have not observational evidence.

2.2. PBHs evolution between formation and merger

Once primordial black holes have formed, depending on some initial factors such as their abundance, mass or spatial distribution, they can evolve in many ways. However, the evolution of interest in this work occurs when they formed binary systems in the early Universe. Although PBHs in these stages are exposed to different forces such as pressure or the expansion of the Universe, if they are close enough, the gravitational force can dominate, giving rise to binary systems of PBHs as we will deal with in chapter 3. Such systems are not stable since, as well as other effects, they loose energy by the emission of gravitational waves. This limits the half-life of these systems, as will be seen in subsection 2.2.1, and ends in a very energetic process called merger, which will be briefly discussed in subsection 2.3.

The formation of binary systems of primordial black holes is not limited to the early Universe. Two primordial black holes could locate in the halos of galaxies close enough that their kinetic energy is lower than their gravitational energy, becoming gravitationally bounded together at present. Such binaries have a very short half-life and quickly merge. However, articles like [21] suggest that this kind of binaries are a subdominant contribution to the total merger rate observed by experiments such as LIGO or Virgo.

The merger rate is obtained by knowing the time it would take for the hypothetical binary systems to collapse, considering the energy loss by the emission of gravitational waves. To get it, we will follow the articles [22] and [23] as well as the book [24].

2.2.1. Coalescence time

Gravitational waves are a consequence of the gravitational field equations of General Relativity, in a similar way to electromagnetic waves and Maxwell's equations. Although we will not do the complete analysis of the gravitational field equations, it is noteworthy that we will use the following approximations :

- The weak field approximation assumes that the curvature caused by the PBH binary is small enough to consider that space-time is flat. Thus, we will use the Minkowski metric to describe it. As a result, it is possible to obtain the linearized equations of the field whose solution corresponds to the gravitational waves.
- As with electromagnetism, the field will depend on the distance between the source and the observer. If we consider that it is far enough away, we could realise a multipolar extension where each of the terms corresponds to the moments that generate the field. This approximation is the so-called Multipole expansion. In the case of gravity, the only momentum to be considered is the quadrupole moment tensor. With this approximation, the calculations are simplified.
- We will assume that black holes are a compact gravitational source with a very short extent compared to the distance in which we will consider the field. It is called as compact-source approximation.

Under these approximations, the quadrupole moment tensor for a slow-moving source with proper density ρ, which is the one that generates the gravitational waves, is given by the following expression

$$I^{ij} = \int \rho(t, \vec{x}) x^i x^j d^3\vec{x} \,. \tag{2.3}$$

The energy and the angular momentum loss by emission of gravitational wave, obtained in [24], are expressed as

$$\frac{dE}{dt} = -\frac{1}{5}\langle [\dddot{J}_{ij} \dddot{J}^{ij}]_r \rangle \quad \frac{dL^i}{dt} = -\frac{2}{5}\epsilon^{ikl}\langle [\ddot{I}_{kj} \dddot{I}^{lk}]_r \rangle \,, \tag{2.4}$$

where

$$J_{ij} = I_{ij} - (1/3) I \delta_{ij} \,, \tag{2.5}$$

corresponds to the reduced quadrupole-moment tensor and I represents their trace and the notation $[]_r$ implies that the expression should be evaluated at the retarded time, i.e. the time it takes for the gravitational force to exert between the PBHs pair, given the finite speed of the interaction.

We can now obtain the energy lost by GW emission in a binary system formed by two PBH with masses M_1 and M_2 following an elliptical orbit in xy plane as shown in Figure 2.2.

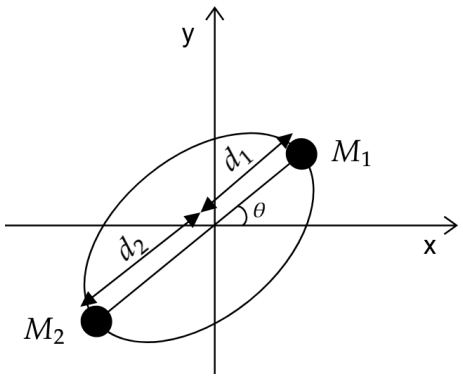

Figure 2.2: A schematic of the binary system with an elliptic orbit to be analysed. The coordinates used are shown.

For simplicity, we will consider the centre of masses as the centre of coordinates. So the coordinates of each of the primordial black holes will be given by

$$\begin{aligned}[x_1^i] &= (d_1\cos\theta, d_1\sin\theta, 0)\\ [x_2^i] &= -(d_2\cos\theta, d_2\sin\theta, 0)\ .\end{aligned} \tag{2.6}$$

Since the centre of coordinates corresponds to the centre of masses, using the reduced mass $\mu = M_1M_2/(M_1+M_2)$ we can relate each of the distances to the total separation d as follows

$$d_1 = \frac{\mu}{M_1}d \quad d_2 = \frac{\mu}{M_2}d\,. \tag{2.7}$$

We will also assume that PBHs have a reduced extension so that they can be considered point masses. Therefore, the proper density will be described by Dirac delta functions δ such as

$$\begin{aligned}\rho(t,\bar{x}) = M_1[\delta(x_1^1 - \frac{\mu}{M_1}d\cos\theta)\delta(x_1^2 - \frac{\mu}{M_1}d\sin\theta)]\delta(x_1^3)\\ +M_2[\delta(x_2^1 + \frac{\mu}{M_2}d\cos\theta)\delta(x_2^2 + \frac{\mu}{M_2}d\sin\theta)]\delta(x_2^3)\ .\end{aligned} \tag{2.8}$$

By integrating this density as in the equation (2.3), it is straightforward to see that the quadrupole-moment tensor is expressed as

$$I^{ij}(t) = d^2\mu\begin{pmatrix}1+\cos 2\theta & \sin 2\theta & 0\\ \sin 2\theta & 1-\cos 2\theta & 0\\ 0 & 0 & 0\end{pmatrix} \tag{2.9}$$

whose reduced quadrupole-moment tensor is

$$J^{ij}(t) = d^2\mu \begin{pmatrix} 1/3 + \cos 2\theta & \sin 2\theta & 0 \\ \sin 2\theta & 1/3 - \cos 2\theta & 0 \\ 0 & 0 & -2/3 \end{pmatrix} . \tag{2.10}$$

If we consider the Kepler's laws to an elliptic orbit, the total distance between the two bodies and the angular velocity $\Omega = \dot{\theta}$ is as follow

$$d = \frac{a(1-e^2)}{1 + e\cos\theta} \tag{2.11}$$

$$\Omega = \frac{[(M_1 + M_2)a(1-e^2)]^{1/2}}{d^2} \tag{2.12}$$

where e is the eccentricity and a is the major semi-axis of the binary. Using these equations the calculation of the third derivative of the reduced quadrupole momentum tensor can be simplified. The derivatives and multiplication are done in [23] whose result is

$$\frac{dE}{dt} = \frac{2}{15}\beta^2\langle(1 + e\cos\theta)^4[12(1 + e\cos\theta)^2 + e^2\sin\theta^2] = \frac{2}{15}\beta^2\langle f(\theta)\rangle \tag{2.13}$$

with

$$\beta^2 = \frac{4M_1^2M_2^2(M_1 + M_2)}{a^5(1-e^2)^5} . \tag{2.14}$$

Where we have considered that the distance between the two black holes is small enough for the retarder time to be negligible.

We will average for one complete period of the elliptical orbit $T = 2\pi/\omega_0$ where $\omega_0^2 = (M_1 + M_2)/a^3$. Hence, it is given by

$$\begin{aligned} \langle f(\theta')\rangle &= \frac{1}{T}\int_0^T dt f(\theta) = \frac{\omega_0}{2\pi}\int_0^{2\pi}\frac{d\theta}{\Omega}f(\theta) \\ &= (1-e^2)^{3/2}\int_0^{2\pi}\frac{d\theta}{2\pi}f(\theta)(1 + e\cos\theta)^{-2} \\ &= 12(1-e^2)^{3/2}\left[1 + \frac{73e^2}{24} + \frac{37e^4}{96}\right] . \end{aligned} \tag{2.15}$$

Replacing in (2.16) the value of (2.15), the average energy lost is given by

$$\frac{dE}{dt} = -\frac{32G^4}{5}\frac{M_1^2M_2^2(M_1 + M_2)}{a^5(1-e^2)^{7/2}}(1 + \frac{72e^2}{24} + \frac{37e^4}{96}) . \tag{2.16}$$

In the same way, we could obtain the value of the lost angular momentum using (2.4) equation. We will take the value obtained in [22], which corresponds to

$$\frac{dL}{dt} = -\frac{32G^4}{5}\frac{M_1^2M_2^2(M_1 + M_2)^{1/2}}{a^{7/2}(1-e^2)^2}(1 + \frac{7e^2}{8}) . \tag{2.17}$$

Once the energy and momentum lost per unit time have been obtained, we will estimate the time required for the binary system to merge. For that aim, we will start assuming the Newtonian approximation, where the orbital parameters are related to energy and momentum as follows

$$E = -\frac{M_1 M_2}{2a}\,, \tag{2.18}$$

$$L^2 = -\frac{M_1^2 M_2^2 a(1-e^2)}{M_1+M_2}\,. \tag{2.19}$$

Therefore, we can get the variation of these parameters as a function of time by using the (2.18) equation as

$$\frac{da}{dt} = \frac{da}{dE}\frac{dE}{dt} = -\frac{64}{5}\frac{M_1 M_2 (M_1+M_2)}{a^3(1-e^2)^{7/2}}(1+\frac{72e^2}{24}+\frac{37e^4}{96}) \tag{2.20}$$

and in a similar way,

$$\frac{de}{dt} = \frac{de}{dL}\frac{dL}{dt} = -\frac{304}{15}\frac{eM_1 M_2 (M_1+M_2)}{a^4(1-e^2)^{5/2}}(1+\frac{121e^2}{304})\,. \tag{2.21}$$

It is possible to combine these two equations, getting

$$\frac{da}{de} = \frac{da}{dt}\frac{dt}{de} = \frac{12a}{19e}\frac{[1+(73/24)e^2+(37/96)e^4]}{(1-e^2)[1+(121/304)e^2]} \tag{2.22}$$

whose solution is given by

$$a(e) = \frac{c_0 e^{12/19}}{(1-e^2)}\left[1+\frac{121e^2}{304}\right]^{870/2299} \tag{2.23}$$

where c_0 is a constant that depends on the initial condition.

Substituting the value derived for the semi-major axis a into equation (2.21), it is reduced to

$$\frac{de}{dt} = -\frac{19\gamma}{12}\frac{e^{-29/19}(1-e^2)^{3/2}}{c_0^4\,[1+(121/304)e^2]^{1181/2299}}\,, \tag{2.24}$$

with

$$\gamma = \frac{64}{5}M_1 M_2 (M_1+M_2)\,. \tag{2.25}$$

Finally, we have obtained the value of the coalescence time solving the (2.24) differential equation and considering that the initial orbital parameters are e_0 and a_0. However, this equation only has an analytic expression when $e_0 \to 1$ or $e_0 \to 0$. In this work, the interesting case is the binaries with high eccentricity, as they have a shorter lifetime since we have to make sure that the binaries merge at least at present time t_0 , i.e. $t_c < t_0$. Hence, the coalescence time corresponds to

$$t_c(a_0, e_0) \approx \frac{768}{425}\frac{a_0^4}{4\gamma}(1-e_0^2)^{7/2}. \tag{2.26}$$

To summarise, the coalescence time will be given mainly by the value of the masses composing the binary system and its orbital parameters. It is larger for small masses and for the large initial major semi-axis.

2.3. Primordial black hole binary merger

As we have discussed in the previous section, after some time the binary systems of primordial black holes get closer together due to the loss of energy and momentum. This approaching causes, by conservation of angular momentum, the angular velocity to increase until they eventually merge into a single black hole. That process is the source of a type of gravitational wave known as an inspiral GW.

The inspiral gravitational wave is divided into three phases: inspiral, merger and ringdown. The inspiral happens when black holes get closer together, causing their angular velocity to become larger. This scenario implies that the gravitational wave emitted in this phase is a wave with a progressively increasing frequency. The merger begins when the PBHs are in the innermost stable circular orbit (ISCO) until they merge. Finally, the ringdown (Rd) is when the merger is over, resulting in a single black hole. All these phases are shown in Figure 2.3

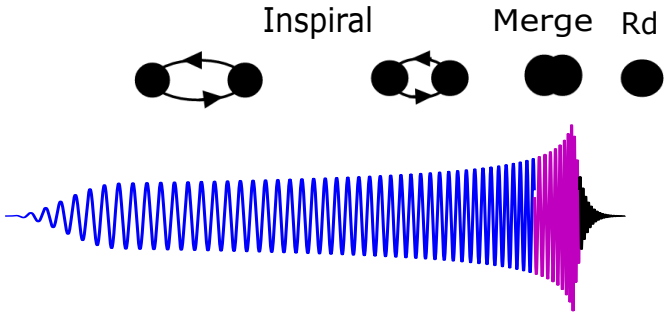

Figure 2.3: The different phases of an inspiral gravitational wave are shown. *Blue:* correspond to the inspiral phases when the PBHs begin to decrease their separation. *Magenta:* represent the merger phases when the PBHs collapse. *Black:* are the ringdown phases and a new huge PBH has been formed. We have used the gravitational wave data of LIGO/Virgo to obtain the signal figure.[25]

These gravitational waves provide us useful information about the binary system such as the chirp mass [2], the effective spin, etc. and we are able to catalogue each of the events in a range of masses. However, it is difficult to know the source of their origin since in the mass range that is detectable by LIGO/Virgo it is indistinguishable whether the black hole is primordial or astrophysical. For that reason, the existence of primordial black holes has not yet been confirmed.

On the other hand, if we assume an initial hypothesis, as the measures are caused by a combination of primordial and astrophysical, this allows us to analyse the concordance between the number of mergers measured by LIGO/Virgo and that determined by the theoretical model. This model will depend, among other things, on the abundance of

[2] In a binary the chirp mass is given by $M = (M_1 M_2)^{5/2}/(M_1 + M_2)^{1/5}$ where M_1 and M_2 are the masses of each black hole.

primordial black holes in the early Universe, so by analysing the agreement we can obtain the constraints on their abundance. These constraints as will be discussed later in chapter 4 will be more or less restrictive depending on the hypothesis taken on the origin of the measured GWs.

Chapter 3

Theoretical estimation of merger rate of Primordial black holes binaries

In this chapter, we will introduce the estimation of the merger rate of primordial black hole binaries. As the estimation of this merger rate will depend on the assumptions we make, we will first review it and its implications in 3.1. In the following section, we will start by estimating the merger rate in the simplest model, in which we will consider a monochromatic mass function. This case, although less realistic, is interesting for academic purposes and it will allow us to establish the basis for the remaining calculations.

Afterwards, once the merger rate is obtained by taking into account the monochromatic mass function in 3.2, we will generalise this case by assuming an extended mass function in 3.3. Finally, we will deal with an approximation of the effect on the merger rate due to the clustered spatial distribution in 3.4. The estimation obtained in these sections will be used for the analysis in the next chapter, where we will get the constraints on the abundance of primordial black holes. Articles [21], [26] and [27] provide a guide for the calculations of the merger rate assuming monochromatic mass function, extended mass function and clustered spatial distribution, respectively.

3.1. Notations and assumptions

As it was discussed in the previous sections, it is necessary to accept some assumptions to obtain the merger rate at present. The main assumptions to be considered are the mass function and the spatial distribution of primordial black holes since the merger rate varies significantly depending on them. The first one is the probability distribution of a black hole to have a certain initial mass. The other is related to the probability of locating another primordial black hole in a volume. In the 3.1.1 and 3.1.2 subsections, we will explain in detail these assumptions and their implications.

Furthermore, we will consider throughout this work that the Universe geometry is described by the Friedmann-Lemaitre-Walker-Robertson metric and the CDM model with

cosmological parameters given by [1].

3.1.1. Initial mass function

In the previous sections, we have explained that depending on the primordial black holes formation mechanism, their masses could be either different or equal. For that reason, we will deal with both assumptions to observe the variation in the constraints in both cases and to consider as many cases as possible.

Primordial black holes mass can be considered as a continuous random variable since it can take any value. So we will define a probability function that describes the continuous probability distribution of masses, which is called the probability density function (PDF). For simplicity, we will name it as the mass function $\psi(M)$, whose main property is that the integral of the whole set of masses has to be equal to one,

$$\int \psi(M)\, dM = 1\,, \tag{3.1}$$

i.e. it is normalised.

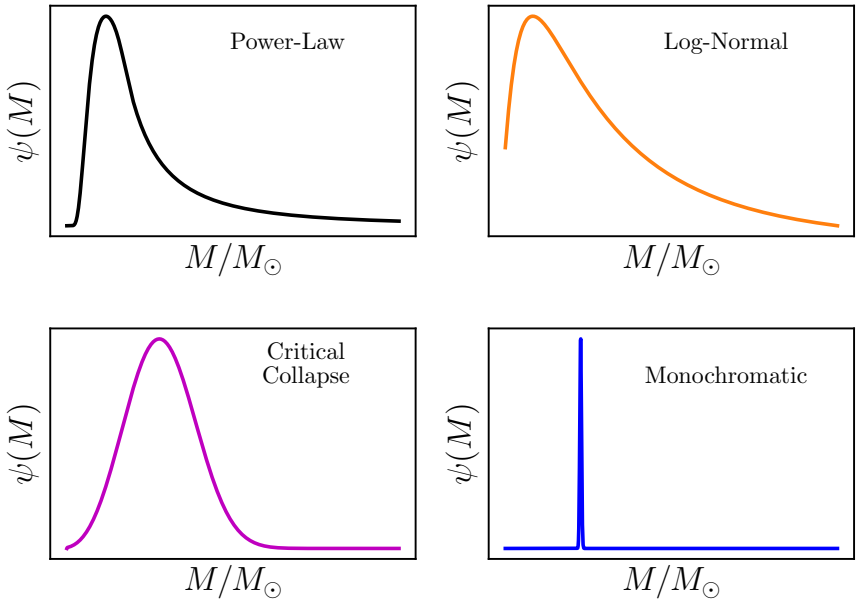

Figure 3.1: Probability distribution functions for the four different mass functions considered in this work.

This mass function will be divided into two cases to cover the major number of formation scenarios since the kind of probability distribution the PBH masses follow is unknown. These mass functions are the monochromatic mass function and the extended mass function, as we have discussed above. Although the formation mechanism or theory that allows such mass distributions is beyond the scope of this work, we have been decided to

focus on three typical extended mass functions, in addition to the monochromatic mass distribution. Therefore, the mass functions to be considered are:

1. **Log-Normal mass function.** Since the PBHs masses depend on the formation mechanism where independent random variables have to be considered, the Central limit theorem could be fulfilled. For that reason, it is common to follow a distribution of this type. The mass function corresponding to this distribution has the following expression,

$$\psi(M \mid \sigma, M_c) \propto \frac{1}{\sqrt{2\pi}\sigma M} \exp\left(-\frac{\log^2(M/M_c)}{2\sigma^2}\right) , \tag{3.2}$$

   where σ is the standard deviation of the mass distribution and M_c is the normal mean mass.

2. **Monochromatic mass function.** This mass function describes a distribution where a single mass value is possible. For that, it is the simplest mass function we can introduce to use in the calculations of the merger rate and it can be used as an approximation in some models where an average mass is used to describe all primordial black holes. This function needs only one parameter, which is the only possible mass of the PBH M_0, and it is given by

$$\psi(M) = \delta_D(M - M_0) , \tag{3.3}$$

   where δ_D is the Dirac delta function.

   Other useful way to define this mass function is to consider a Log-Normal mass function as (3.2) with a very low sigma value $\sigma \approx 0.05$ and $M_c = M_0$. This approximation is possible for all extended mass functions, but the Log-Normal is the simplest case. Also, this approximation produces a change in the merger rate results. However, it could be valid for an estimation.

3. **Power-law mass function.** It is another of the most common functions to describe the probability distribution, as it considers the possible lower limit of masses predicted by some of the formation models. Furthermore, we will introduce a function to smooth the shape of the function to have better-behaved, called the smoothing function S. This function is defined by

$$S\left(M \mid M_{min}, \delta_m\right) = \begin{cases} 0 & M < M_{min} \\ \left[g\left(M_{min}, M, \delta_m\right) + 1\right]^{-1} & M_{min} < M < M_{min} + \delta_m \\ 1 & M_{min} + \delta_m < M \end{cases} \tag{3.4}$$

   with

$$g\left(M_{min}, M, \delta_m\right) = \exp\left(\frac{\delta_{\mathrm{m}}}{\mathrm{M} - \mathrm{M}_{\mathrm{min}}} + \frac{\delta_{\mathrm{M}}}{\mathrm{M} - \mathrm{M}_{\mathrm{min}} - \delta_{\mathrm{m}}}\right) ,$$

where δ_m is an extra parameter, which refers to the extent of smoothing and has units of solar mass, and M_{min} is the lower mass cut-off. Therefore, the Power-law mass function, whose power index α, is given by

$$\psi\left(M \mid \delta_m, \alpha\right) \propto M^{-\alpha} S\left(M \mid M_{min}, \delta_m\right) \ . \tag{3.5}$$

The minimum mass is considered as $M_{min} \approx 3\ \mathrm{M}_\odot$ [28]. This mass function will consequently be given by two parameters.

4. **Critical Collapse mass function.** It is similar to a Power-Law function mass except for huge masses, which has an exponential upper cut-off at M_f. This mass function is typical since black holes are considered to have been formed by a critical collapse where we will expect that the most to have the critical mass, and there is an exponential decay for higher masses.[29] This function is given by

$$\psi(M \mid \beta, M_f) \propto M^{\beta} \mathrm{exp}\left(-\left(\mathrm{M}/\mathrm{M_f}\right)^{\beta}\right) \tag{3.6}$$

where β is the power-law index, whose common value is $\beta = 2.85$. [30]

3.1.2. Initial spatial distribution

As happens with the mass distribution, the initial spatial distribution depends on the formation mechanism and the perturbations that generate the PBHs. In this work, we will deal with the uniform spatial distribution and the clustered spatial distribution. We will consider both distributions since they are possible in many formation scenarios. In the following subsections, we will determine the differential probability of locating a black hole in a given volume.

3.1.2.1. Uniform spatial distribution

Before starting with the calculation of the probability of locating a primordial black hole between the volume V and $V + \delta V$, we will consider in this case that the initial distribution is uniform and satisfies:

- The expected number of PBH depends only on the volume. In addition, the volume it is expected to find a PBH is considered as V_0.
- The probabilities of locating a primordial black hole in two different regions are independent.

Since it satisfies these conditions, we will start by defining the differential probability of locating a primordial black hole in $V + \delta V$ as

$$dP(V + \delta V) = \bar{P}(V) P(\delta V) \, , \tag{3.7}$$

where $P(\delta V)$ is the probability to find PBH in the infinitesimal volume and $\bar{P}(V)$ is the probability of not find the first neighbour PBH in a volume V.

This probability of non-locating the first neighbour PBH in V can be obtained by using the following expression

$$\bar{P}(V+\delta V) = \bar{P}(V)(1-P(\delta V)) \text{ with } \mathrm{P}(\delta \mathrm{V}) = \mathrm{dV}/\mathrm{V}_0\,. \tag{3.8}$$

If we now consider that the probability of non finding in the null volume is one, the solution of (3.8) equation is given by

$$\bar{P}(V) = e^{-V/V_0}\,. \tag{3.9}$$

Hence, substituting (3.9) into (3.8) equation and assuming that $\delta V \to 0$ we obtain that

$$\frac{dP}{dV} = \frac{1}{V_0} e^{-V/V_0} \tag{3.10}$$

3.1.2.2. Clustered spatial distribution

There are some formation scenarios where primordial black holes form in clusters. It is common in the study of these clusters to consider a function called a two-point correlation. This function will describe the excess probability of finding the nearest neighbour primordial black hole when they are in a cluster, $\zeta(V)$. So, as the value of the two-point correlation function increases, the effect of the lumpiness and the non-independence of the location of PBHs will be stronger.

To generalise the probability obtained in the previous section taking into account the two-point correlation function, we will consider that the number of black holes in a volume V will be given by $N = n\int_V (1+\xi(s))d^3\mathbf{s}$.[31] We will therefore rewrite the (3.10) equation as

$$\frac{dP}{dV} = \frac{(1+\xi(V))}{V_0} \exp\left(-\frac{1}{\mathrm{V}_0}\int_{\mathrm{V}} (1+\xi(\mathrm{s}))\mathrm{d}^3\mathbf{s}\right)\,. \tag{3.11}$$

The two-point correlation function will depend on some factors such as the formation of black holes, their mass distribution or their abundance. However, given the limitations of this work, we will consider the ideal case in which the correlation function does not depend on the comoving volume and hence, is constant $(\xi+1) \approx \zeta$ in cluster radius $\tilde{x}$. So, the (3.11) equation can be simplified as

$$\frac{dP}{dV} = \frac{\zeta}{V_0} \exp\left(-\frac{\mathrm{V}\zeta}{\mathrm{V}_0}\right)\,, \tag{3.12}$$

where we will refer to ζ as a clustering parameter.

The effect of clustering will be more or less noticeable in the result of the merger rate calculation, depending on the value of parameter ζ, where $\zeta = 1$ corresponds to the initial uniform distribution. When the clustering parameter is close to one, its effect on the merger rate will be weaker than the change between any parameter of the mass function, as shown in [27].

Although the probability obtained in this subsection is approximate, it will be useful to compare how much the clustering effect can affect our estimation of the merger rate.

3.2. Merger rate estimation considering monochromatic mass function and initial uniform spatial distribution

In the section, we will obtain the merger rate assuming a monochromatic mass function and a uniform spatial distribution of PBHs. Despite this is an unrealistic model due to it is no-possible to produce a monochromatic mass function, it is a good starting point for the rest of the merger rate calculations. Furthermore, we will compare this merger rate with the merger rate given by LIGO/Virgo in the next chapter.

3.2.1. Basic concepts

Let us begin by assuming that the primordial black hole binaries decouple from the Hubble flow at the early radiation era. It means that the gravitational force exerted by each PBH is stronger than the force of the Universe expansion, as we will discuss below. Furthermore, we have to consider that the PBH density could constitute only a fraction of the total dark matter density and therefore, the value of the PBHs abundance is given by $f_{\rm PBH} \approx f/0.85$, where we consider that $\Omega_{\rm DM} \approx 0.85\,\Omega_{\rm m}$. Therefore, the mean value of the comoving separation between two members of a PBH pair $\bar{x}$ at this moment is expressed as

$$\bar{x} \equiv \left(\frac{3M}{4\pi f \rho_{\rm eq}}\right)^{1/3}, \tag{3.13}$$

where M is the mass of all the primordial black holes, $\rho_{\rm eq}$ is the density at equality and it is assumed that the volume is spherical.

However, we will deal with the dimensionless variable X for simplicity of calculation. This variable will give us an idea of the comoving distance between the two black holes x compared to the mean value. It is given by

$$X \equiv \left(\frac{x}{\bar{x}}\right)^3 . \tag{3.14}$$

The merger rate will depend on the angular momentum L and the initial distance between the black holes, considered as the major semi-axis a because of having an elliptical orbit. As happens with the comoving separation, we will deal with the dimensionless angular momentum j that is expressed as

$$j \equiv l/\sqrt{2Ma} = \sqrt{1-e^2}\,, \tag{3.15}$$

where e is the eccentricity. We have used in the last equality step the definition of the angular momentum per unit reduced mass l, which is

$$l = 2L/M^2 = (2Ma(1-e^2))^{1/2}\,. \tag{3.16}$$

Another factor to consider is the possibility that if primordial black holes do not constitute all the dark matter. In that case, the remaining dark matter density perturbation could

exert an extra tidal force that changes the initial conditions of PBHs. The value of this perturbation obtained in [32] is given by

$$\sigma_{eq}(M) \simeq 0.0061 \left(\frac{M}{\mathrm{M}_\odot}\right)^{7/1200} \left[1 - 0.06 \log\left(\frac{M}{\mathrm{M}_\odot}\right)\right]^{3/2} , \tag{3.17}$$

where we consider $n_s = 0.965 \pm 0.004$.[1] This factor causes suppression in the merger rate since it disturbs the initial orbital parameters, and we will approximate this value for the range of mass $(10^{-4} - 10^3)\mathrm{M}_\odot$ as $\sigma_{eq} \approx 0.005$.

3.2.2. Initial major semi-axis

Once we have defined the basics concepts, we will deal with the description of the initial semi-axis major a for PBH binaries. Therefore, we have to solve the equation of motion of primordial black holes by considering their gravitational attraction and the force exerted by the Hubble flow. Using a Newtonian approximation of gravitational force, the proper separation between the PBHs r evolves as

$$\ddot{r} = \frac{d}{d\tau} v_H + F_{grav} = -(\dot{H} + H^2) r + \frac{2M}{r^2} \frac{r}{|r|} , \tag{3.18}$$

where τ is the proper time and v_H is the Hubble velocity given by the Hubble law $v_H = Hr$.

In order to simplify the motion equation (3.18), we will define the scale factor normalised to the unit of the scale factor at equality era, $s = a/a_{eq}$. Hence, the Hubble constant in the function of the normalised scale factor is expressed as

$$H(s) = \left(\frac{8\pi\rho_{eq}}{3}\right)^{1/2} h(s) , \tag{3.19}$$

where $h(s)$ is the normalised Hubble constant assuming that the density parameters of curvature and dark energy are negligible and it is given by $h(s) = (s^{-3} + s^{-4})^{1/2}$.

Let us now rewrite the equation (3.18) in terms of normalised scale factor instead of the proper time and considering the variable $\chi \equiv r/x$. Giving as a result

$$\ddot{\chi} + \frac{sh' + h}{s^2 h}(s\dot{\chi} - \chi) + \frac{1}{\lambda} \frac{1}{(sh)^2} \frac{1}{\chi^2} \frac{\chi}{|\chi|} = 0 , \tag{3.20}$$

$$\text{with} \quad \lambda \equiv \frac{4\pi\rho_{\mathrm{eq}} \mathrm{x}^3}{3\mathrm{M}} = \mathrm{X/f} , \tag{3.21}$$

where we have used the (3.14) and (3.19) equations and λ is a dimensionless parameter.

Since in the initial formation era the PBHs motion is dominated by the Hubble flow $\chi(s) \approx s$, the boundary conditions are given by

$$\chi(0) = 0 \quad \dot{\chi}(0) = 1 . \tag{3.22}$$

We will assume that the PBHs decouples from the Hubble flow in the early radiation-domination era, i.e. $s \ll 1$. It implies that $\lambda \ll 1$ and we can approximate the normalised Hubble constant as $h(s) \approx s^{-2}$. The (3.20) equation could be rewritten as

$$\ddot{\chi} - \frac{1}{s^2}\left(s\dot{\chi} - \chi\right) + \frac{1}{\lambda}\frac{s^2}{\chi^2}\frac{\chi}{|\chi|} = 0\,. \tag{3.23}$$

We will take the numerical solution of this differential equation numerically from [21]. They obtain that the binary decouples from the Hubble flow at $s \approx \lambda/3$ as we had assumed. Also, they obtain that the solution oscillated with amplitude $|\chi| \approx 0.2\,\lambda = r/x$ where r corresponds to twice the value of the PBH binary semi-major axis. Therefore, the initial semi-major axis is given by,

$$a \approx 0.1\lambda x = 0.1\left(\frac{3M}{4\pi\rho_{eq}}\right)^{1/3}(X/f)^{4/3}\,, \tag{3.24}$$

where we have used (3.13) and (3.21) equations in the last equality.

3.2.3. Initial angular momentum

The PBH binaries, once decoupled from the Hubble flow, will be subjected to the gravitational force exerted by the rest of the PBHs and by the large density perturbations at this time. As the exerted forces to the binary have different directions and intensities, we will account that these forces behave like a local tidal field $\mathbf{T}$[1].

It is now noteworthy to point out that the effect of the local tidal field in the binary's energy is negligible. Since the potential energy depends on the comoving distance and the initial comoving separation of the binary are small comparing with the mean separation $x \ll \bar{x}$. Therefore, we will only consider the effect of this tidal field on angular momentum.

We will assume that the local tidal field is $\mathbf{T} \approx \mathbf{T_{eq}}\, s^{-3}$, where $\mathbf{T_{eq}}$ is the local tidal field at the equality. This assumption could made because if so since if we consider that the rest of the PBH is far, the tidal field would decrease with the scaling factor as $\mathbf{T} \sim \rho_{\rm PBH} \propto s^{-3}$. Similarly, it is the case of linear perturbations of the matter density, due to the dependence of the local tidal field on the matter density as $\mathbf{T} \propto s^{-3}\delta_m$, where δ_m is the size of the perturbation. During the deep radiation-domination era, the matter density perturbations had a growth slow enough to assume it is as constant.

Given the local tidal field, we will obtain the force exerted to the binary as $\mathbf{F} = \mathbf{T}\cdot\mathbf{r}$. Hence, the angular momentum is given by

$$\begin{aligned} l = \int dt(\mathbf{r}\times[\mathbf{T}\cdot\mathbf{r}]) = \int ds\frac{dt}{ds}(\mathbf{r}\times[\mathbf{T}\cdot\mathbf{r}]) = \int \frac{ds}{\dot{s}}\chi^2(\mathbf{x}\times[\mathbf{T_{eq}}\cdot\mathbf{x}]) = \\ \left(\frac{3}{8\pi\rho_{eq}}\right)^{1/2}\int\frac{ds}{h(s)s}\frac{\chi^2}{s^3}(\mathbf{x}\times[\mathbf{T_{eq}}\cdot\mathbf{x}]) \approx 0.3\,(\mathbf{x}\times[\mathbf{T_{eq}}\cdot\mathbf{x}])\left(\frac{3\lambda^2}{8\pi\rho_{eq}}\right)^{1/2}\,, \end{aligned} \tag{3.25}$$

[1] We use the letters in boldface type to represent matrix notation.

where we have used (3.19) equation in order to simplify the expression and the resolution of the integral has been adopted from [21], where they assumed that $\lambda \ll 1$ (i.e. $h(s) \approx s^{-2}$).

Once we have computed the value of the initial angular momentum, we can obtain the reduced angular momentum using the equations (3.25) and (3.28) which is expressed as

$$\mathbf{j} \approx 0.5 x^3 \, \hat{x} \times \left[\frac{\mathbf{T_{eq}} \hat{x}}{M} \right] , \tag{3.26}$$

where $\hat{x} = \mathbf{x}/\left|x\right|$.

To obtain the reduced angular momentum, we have to estimate the value of the local tidal field at equality. As discussed previously, this field is provided by two sources, the rest of the PBHs and the linear density perturbations. On both occasions, we will consider the Newtonian approximation due to the comoving distance between all the PBHs, and the binary y is very large compared to the comoving distance x. The tidal field generated by all PBHs is given by the expression,

$$T^{ij}_{eq} = \sum_{p}^{N} \frac{(3\hat{y}^i_P \hat{y}^j_P - \delta^{ij}) M}{y^3_P} , \tag{3.27}$$

where we use the superposition principle to obtain the total tidal field and N corresponds to the total number of PBHs.

Hence, we can compute the reduced angular momentum substituting in the (3.26) the value of (3.27) as follow

$$\mathbf{j} \approx 1.5 \sum_{p}^{N} \frac{x^3}{y^3_p} (\hat{x} \cdot \hat{y_p})(\hat{x} \times \hat{y_p}) = 1.5 \sum_{p}^{N} \frac{x^3}{y^5_q} y_{q\parallel} y_{q\perp} . \tag{3.28}$$

It is possible to compute the probability distribution of j since there are certain values of j are more probable. We have done the explicit calculation in appendix A, whose result is

$$j \frac{dP}{dj}|_X = P(j/j_X) \tag{3.29}$$

$$P(\gamma) \equiv \frac{\gamma^2}{(1+\gamma^2)^{3/2}} , \tag{3.30}$$

where $j_X = 0.5X$. This probability distribution accounts for torques by all PBHs. Therefore, we could obtain not only the value of reduced angular momentum but also the probability distribution.

As already mentioned, there exists other possible contribution to the tidal field that is produced by large-scale linear density perturbation $T_{ij} \approx \delta_m s^{-3}$. To estimate this contribution, we will assume that the linear density perturbation has a Gaussian amplitude.

Therefore, on the basis of the result of [21], the reduced angular momentum by a linear density perturbations is

$$\langle j^2 \rangle^{1/2} = \sqrt{0.3}\frac{\sigma_{eq} X}{f} \approx 0.5\frac{\sigma_{eq}}{f} X \, . \tag{3.31}$$

The reduced angular momentum corresponds to the convolution of the probability distribution of all the PBHs and the large linear density perturbation. However, other simple way to solve it is by the equation (3.29) with the characteristic value

$$j_X \approx 0.5(1 + \sigma_{eq}^2/f^2)^{1/2} X \, . \tag{3.32}$$

We will obtain the initial reduced angular momentum and its probability distribution. These contributions to the angular momentum allow PBH binaries to have stability, increasing the possibility of their existence at present.

3.2.4. Differential probability distribution of the time of merger

The primordial black hole merger rate depends on the probability of PBH merger occur in an interval of time $[t, t + dt]$,i.e. the differential probability distribution of the merger rate dP/dt. In this section, we will obtain it considering the characteristic initial properties of the PBH binaries.

We will start considering the differential probability distribution of $(X; t)$, which it is possible to write in terms of the reduced angular momentum using the chain rule as

$$\frac{d^2 P}{dX dt} = \frac{dP}{dX}\frac{dj}{dt}\left.\frac{dP}{dj}\right|_X \, . \tag{3.33}$$

To get the reduced angular momentum in terms of time, we have to consider the coalescence time. It is time that the PBH binary takes for collapse by the energy loss due to the emission of gravitational waves. The coalescence time expression was determined in 2.2.1, and it is given by

$$t = (3/170)(a^4/M^3)(1 - e^2)^{7/2} = (3/170)(a^4/M^3) j^7 \, , \tag{3.34}$$

where we assume that the initial eccentricities are close to unity and the (3.15) equation has been used.

After substituting the value of the semi-major axis from the previous sections in the (2.26) equation, we have the following expression of the reduced angular momentum in terms of the dimensionless variable X and the time

$$j(t, X) = \left(\frac{170}{3}\frac{M^3 t}{a^4}\right)^{1/7} = \left(\frac{170}{3}\frac{M^3 f^4 t}{(0.1\bar{x})^4 X^{16/3}}\right)^{1/7} \, . \tag{3.35}$$

Once obtained the reduced angular momentum in terms of the time and assuming an initial uniform spatial distribution (see our development at 3.1.2 subsection), the (3.33) equation is rewritten as

$$\frac{d^2 P}{dX dt} = \frac{1}{7t} e^{-X} P(\gamma x) \, . \tag{3.36}$$

where it has been derived the (3.35) respect the time and we have used to simplify the (3.29) function with $\gamma x \equiv j(t;X)/jx$. Also, the (3.14) equation is used to simplify the differential probability of X, given by (3.10) equation[2].

Before computing the differential probability distribution of the time merge is worthy, as we have discussed previously, to get the characteristic initial properties of PBH binaries. Specially, we will deal with the characteristic [3] dimensionless separation X_* since the other properties depend on it.

Hence, considering that $X_* \ll 1$ so $e^{-X} \approx 1$ and using the Bayes' theorem, the differential probability distribution of X is expressed as follows

$$\frac{dP}{dX}\left[\frac{dP}{dt}\right] \propto \frac{dP(\gamma_{X_*})}{dX}\frac{\gamma_X}{dX}\,. \tag{3.37}$$

The characteristic dimensionless separation X_* corresponds to the value of X that maximises their differential probability distribution, i.e. the value that satisfies the following equation

$$\frac{\partial}{\partial X}\left[\frac{dP}{dX}\right]_{X_*} \propto \frac{\partial P(\gamma x_*)}{\partial X}\frac{d\gamma x}{\partial X} = 0\,. \tag{3.38}$$

Since $(\dot{\gamma x}) \neq 0$ then $\dot{P}(\gamma x_*) = 0$ and it is satisfied when $j(t;X_*)/j_{x_*} = \sqrt{2}$. Solving this equation and using (3.32) and (3.35), we obtain the following characteristic dimensionless value

$$X_* \approx 0.032 f M^{5/37}(f^2+\sigma_{eq}^2)^{-21/74}\left(\frac{t}{t_0}\right)^{3/37}\,. \tag{3.39}$$

Back to the calculation of dP/dt, now we only have to use that $\gamma x \propto X^{-37/21}$ and $\gamma x_* = \sqrt{2}$ to compute the following integral as

$$\begin{aligned}\frac{dP}{dt} &= \int dX \frac{d^2P}{dXdt} = \frac{1}{7t}\int dX P(\gamma x)\\ &= \frac{21}{259t}\frac{X_*}{\sqrt{2}}\int d\gamma(\gamma/\sqrt{2})^{-58/37}P(\gamma) \approx 0.0843\frac{X_*}{t}\,,\end{aligned} \tag{3.40}$$

where we have computed the last integral numerically ourselves.

3.2.5. Merger rate

This section aims to get the merger rate per unit volume at present $\mathcal{R}(t_0)$. For this purpose, the probability of an event occurring at the current time has been calculated in the previous sections and now we only have to introduce the number of PBHs per unit volume $dN_{\rm PBH}/dV$.

[2] As $V_0 = (4\pi/3)\bar{x}^3$ and $V = (4\pi/3)x^3$, the ratio between them are $V/V_0 = (x/\bar{x})^3 = X$.

[3] We so-called as characteristic to the most probable value. In the case of X_*, corresponds to the most probable initial distance between PBHs.

Since the number of PBHs per unit volume can be estimated by

$$\frac{dN_{\rm PBH}}{dV} = \frac{1}{2} f \frac{\rho_m}{M} \,, \tag{3.41}$$

where $f\rho_m$ represents the density of PBHs and we add $1/2$ factor to avoid double counting since they are binary systems.

The merger rate per volume unit is given by

$$\begin{aligned} \mathcal{R}(t) = \frac{dN_{\rm PBH}}{dV dt} \approx 0.0421 \frac{X_* f \rho_m}{Mt} \\ \approx (3.69 \cdot 10^6) \rho_m f^2 M^{-32/37} (f^2 + \sigma_{eq}^2)^{-21/74} \left(\frac{t}{t_0}\right)^{-34/37} \,, \end{aligned} \tag{3.42}$$

where we have used (3.39) and (3.40) equations. Furthermore, we have consider that $\rho_m = 3.77 \cdot 10^{19}\ \mathrm{M}_\odot/\mathrm{Gpc}^3$ and $t_0 = 13.78$ Gyr.[1]

Once we have obtained the estimated merger rate per volume at present time, we can compare it with the LIGO/Virgo data. This comparison will be done in detail in chapter 4. However, we could see some properties in Figure 3.2. The first property, which we will expect, is that the merger rate increases as the abundance of primordial black holes increases. This property is due to the fact that if initially there is a large abundance of PBHs, more black holes will likely form binary systems since the distance between them would be smaller. On the other hand, we will expect that there is a small kink around $f_{\rm PBH} = 10^{-2}$. This kink is since as the black hole abundance decreases, the effect of linear density perturbations on the tidal forces becomes more important than given by the rest of the PBHs.

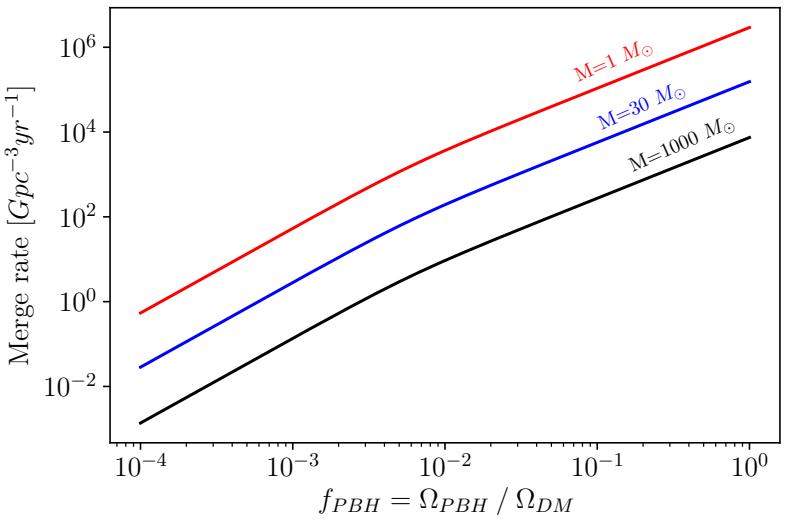

Figure 3.2: The merger rate per volume unit as a function of the DM fraction of PBHs $f_{\rm PBH}$ at present. *Solid line:* merger rate per volume units for three different PBH masses (10, 30, 1000) $\mathrm{M}_\odot$.

3.3. Generalisation of the merger rate for an extended mass function

In the previous section, we have dealt with the simplest merger rate calculations where we have considered that all PBHs have the same mass. Nevertheless, to obtain a more realistic merger rate we have to consider an extended mass function. For that, we will generalise the calculations carried out in section 3.2. Moreover, after the general estimation, we will observe it for different mass functions and parameters described in 3.1.1.

3.3.1. Changes in the initial properties of PBH binaries

The distance given by (3.13) corresponds to the average comoving separation between two neighbours PBHs with the same mass. However, we have to consider not only the two PBHs neighbours will have different masses but also each mean separation between two PBH with the mass M_i depend on their abundance as

$$\bar{x}_i = \left(\frac{3M_i}{4\pi\rho_{eq} f\psi(M_i)}\right)^{1/3} dM_i^{-1/3}\,, \tag{3.43}$$

which is similar to the (3.13) equation except we will consider that the abundance is given by the extended mass function as $dn = \psi(M)dM$. Hence, we will estimate the average distance between two PBHs neighbours with masses M_i and M_j as

$$\langle x_{ij}\rangle = (\bar{x}_i^{-3} + \bar{x}_j^{-3})^{-1/3} = \mu_{ij}^{1/3}\bar{x}_{ij}\,, \tag{3.44}$$

with

$$\mu_{ij} = \frac{2M_iM_j}{M_t(\psi(M_i)M_j + \psi(M_j)M_i)dM}, \tag{3.45}$$

$$\bar{x}_{ij}^3 = \frac{3M_t}{8\pi\rho_{eq} f}\,, \tag{3.46}$$

where $M_t = M_i + M_j$ is the total mass of the system and we use that M_i and M_j are independent and identically distributed random variables, i.e. it is possible to consider equal dM_i and dM_j . This set of equations is generally valid except when the two PBHs have the same mass. In this case, we have to re-scale the abundance by a factor of 1/2, i.e. $(1/2)\psi(M)dM$.

Once generalised the average distance between two PBHs, we will consider the results of (3.20) equation taking into account that the gravitational force now depends on the total mass M_t. It implies that the value of the parameter λ and the semi-major axis are now given by

$$\lambda = \frac{8\pi\rho_{eq}x^3}{3M_t} = \frac{X}{f}\,, \tag{3.47}$$

$$a \approx 0.1\lambda x = 0.1\left(\frac{3M_tX^4}{8\pi\rho_{eq}f^4}\right)^{1/3}\,. \tag{3.48}$$

Concerning now the reduced angular momentum, as we discussed previously it is given by the local tidal field which depends on the gravity force, i.e. on the mass. Therefore, the torque provided by both PBHs and linear density perturbation will be different if we consider that the PBHs have different mass and abundance.

Let us now start from the result of (3.25) equation of the angular momentum. If we substitute the new value of λ and we use the (3.15) equation considering that the total mass is now M_t, we get the reduced angular momentum expressed as follow

$$\mathbf{j} \approx \frac{0.3}{\sqrt{0.1x\lambda M_t}} \left(\frac{3\lambda^2}{8\pi\rho_{eq} M_t} \right)^{1/2} \approx \frac{x^3}{M_t} (\hat{x} \times [\mathbf{T_{eq}} \cdot \hat{x}]) \,, \tag{3.49}$$

so we can use the (3.27) equation considering that the PBHs, which generated by the tidal field, have a different mass M_l to get the reduced angular momentum as

$$\mathbf{j} \approx 3 \frac{M_l}{M_t} \frac{x^3}{y^3} (\hat{x} \cdot \hat{y})(\hat{x} \times \hat{y}) \,. \tag{3.50}$$

As we can see in the appendix A, if we consider the reduced angular momentum given by (3.50), we have the same probability distribution of (3.29) and the characteristic reduced angular momentum, i.e. $j_X = 0.5X$. Note that the value of $\bar{x}$ does not correspond to that of the previous section.

Hence, considering the both effects, the characteristic reduced momentum is given by

$$j_X \approx 0.5(1 + \sigma_{eq}^2/f^2)^{1/2} X \,. \tag{3.51}$$

where X is now different since the mean separation between PBHs are now given by (3.43).

3.3.2. Generalisation of the differential probability distribution of the merger rate for the case of an extended mass function.

As noted in (3.2.4), the differential probability distribution of $(X;t)$ depends on the derivative of the reduced angular momentum respect to the time. Consequently, we will obtain this reduced angular momentum in the function of time using their dependence with the coalescence time. For this case, the coalescence time calculated in 2.2.1, considering that the value of γ is now different, is expressed as

$$t = \frac{3}{85} \frac{a^4}{M_i M_j M_t} j^7 \,, \tag{3.52}$$

and therefore, by substituting the value of the semi-major axis (3.47) we have that the reduced angular momentum is

$$j = \left(\frac{85}{3} \frac{M_i M_j M_t f^4 t}{(0.1\bar{x})^4 X^{16/3}} \right)^{1/7} . \tag{3.53}$$

Considering the reduced angular momentum and assuming that the spatial distribution of PBHs is uniform, we will get a similar differential probability distribution of $(X;t)$ expression using the (3.33) equation. However, the dimensionless spatial parameter X now is given by $\tilde{X} = x^3/\langle x_{ij}\rangle^3 = X/\mu$. We have to rewrite the (3.40) equation as

$$\frac{dP}{dt} = \int d\tilde{X} \frac{dP}{d\tilde{X}dt} = \frac{1}{7t\mu} \int dX e^{-X/\mu} P(\gamma_X) \,, \tag{3.54}$$

where $\gamma_X = j(X;t)/j_X$.

To resolve the last integral done in (3.40), we have to get the most probable initial dimensionless separation X_*. As this is the same problem as discussed previously, we will take its results $j(t_0; X_*)/j_x = \sqrt{2}$ and with them, using both (3.53) and (3.51), it has been found that the characteristic dimensionless separation is

$$X_* \approx 0.032\, M_t^{-1/37} f (f^2 + \sigma_{eq}^2)^{-21/74} (M_i M_j)^{3/37} \left(\frac{t}{t_0}\right)^{3/37} \,. \tag{3.55}$$

We will note that we will obtain the same result as (3.40) except of the factor μ^{-1}, i.e. the differential probability distribution of merger rate is given by

$$\frac{dP}{dt} \approx 0.0843 \frac{X_*}{\mu t} \,. \tag{3.56}$$

3.3.3. Merger rate

We have to obtain now the number of PBHs per volume unit considering an extended mass function. As the number density depends on the PBHs abundance of each of the black holes, we can assume it is the minimum abundance between the two possible cases. An extreme example of that is if there is a zero probability that a black hole with a particular mass exists, the probability of forming such a binary system where one of the black holes has that mass is also zero. Thus, the number density of primordial black holes would be given by

$$\frac{dN_{\rm PBH}}{dV} \approx f \rho_m \min\left(\frac{\psi(\mathrm{M_i})}{\mathrm{M_i}}, \frac{\psi(\mathrm{M_j})}{\mathrm{M_j}}\right) \mathrm{dM} \,. \tag{3.57}$$

The differential merger rate per volume and time units at present assuming an extended mass function and an initial uniform spatial distribution is

$$\begin{aligned} \frac{d\mathcal{R}(t)}{dM_i dM_j} \approx{}& (3.7 \cdot 10^6)\, f^2 (f^2 + \sigma_{eq}^2)^{-21/74} (M_i + M_j)^{36/37} (M_i M_j)^{3/37} \\ & \cdot \left(\frac{\psi(M_i)}{M_i} + \frac{\psi(M_j)}{M_j}\right) \min\left(\frac{\psi(\mathrm{M_i})}{\mathrm{M_i}}, \frac{\psi(\mathrm{M_j})}{\mathrm{M_j}}\right) \left(\frac{\mathrm{t}}{\mathrm{t_0}}\right)^{-34/37} \,, \end{aligned} \tag{3.58}$$

where it has used the density matter of Universe value $\rho_m = 3.77 \cdot 10^{19}\ \mathrm{M_\odot/Gpc^3}$. It is easy to show that once we substitute the monochromatic mass function in (3.58), we obtain (3.42).

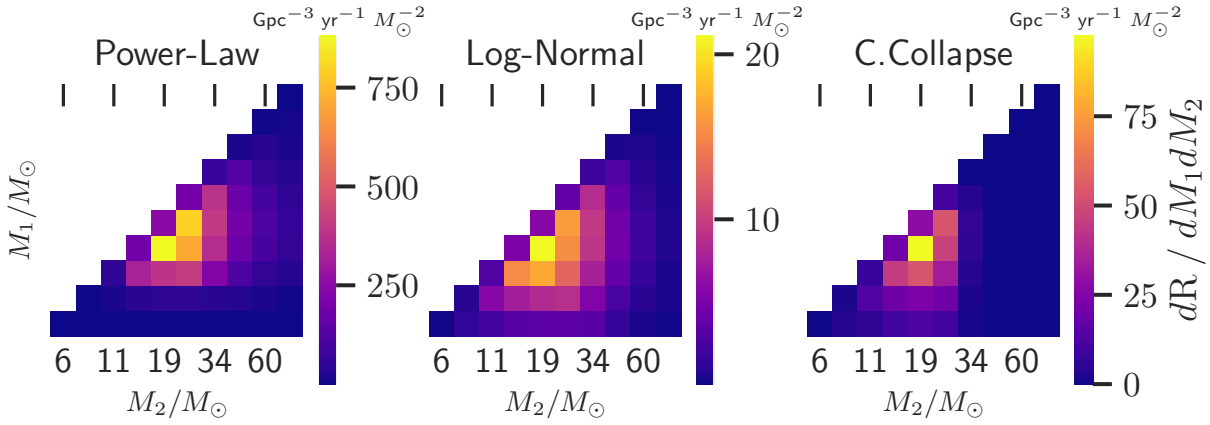

Figure 3.3: The differential merger rate of PBH binaries in function of each PBH masses. For the case of the Power-Law mass function, $\alpha = 2.2$ and $\delta = 30\,\mathrm{M}_\odot$ parameters have been considered. To the case of Log-Normal has been used $\sigma = 0.6$ and $M_c = 30\,\mathrm{M}_\odot$. For the Critical Collapse mass function, $\beta = 2.85$ and $M_c = 20\,\mathrm{M}_\odot$.

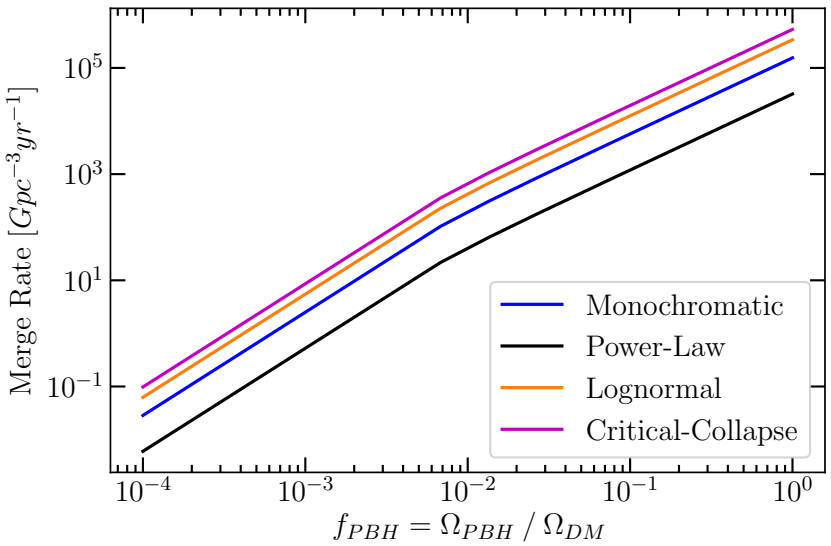

Figure 3.4: The merger rate per volume unit as function of the DM fraction of PBHs f_{PBH} at present time. *Black solid line:* the merger rate for Power-Law mass function with parameters $\alpha = 2.2$ and $\delta = 20\,\mathrm{M}_\odot$. *Orange solid line:* the merger rate for Log-Normal mass function with parameters $\sigma = 1$ and $M_c = 30\,\mathrm{M}_\odot$. *Magenta solid line:* the merger rate for Critical Collapse mass function with the parameters $\beta = 2.85$ and $M_c = 30\,\mathrm{M}_\odot$ *Blue solid line:* the merger rate for monochromatic mass function of $M_0 = 30\,\mathrm{M}_\odot$.

On the other hand, we will see in Figures 3.3 and 3.4 the value of the differential merger rate for different mass pairs and the total merger rate at present. We have obtained Figure 3.3 considering ten values of each mass M_1 and M_2 and using both the

mass function described in 3.1.1 and the differential merger rate equation (3.58). In Figure 3.4, we have integrated numerically in the mass range $M_1, M_2 \in [3, 100]\,\mathrm{M}_\odot$ the (3.58) equation to obtain the total merger rate for each mass function. We have use sofware programming to do it.

As we have discussed in the previous section, the merger rate begins to be dominated by the linear density perturbation value σ_{eq}. This characteristic property is easy to see in Figure 3.4. Furthermore, it is noteworthy that despite having different mass functions, the merger rate does not diverge much.

3.4. Simplified estimation of the merger rate considering clustered spatial distribution with an extended mass function

Finally, we will obtain the merger rate assuming an initial clustered spatial distribution. For that, we will consider our own clustered spatial distribution approximation obtaining in 3.1.2. Although it is only an approximation, we could see how change the merger rate when we assume the clustering effect. In addition, we will start from the generalised estimation of the merger rate with an extended mass function computed above.

The clustered spatial distribution assumption implies that the mean distance between primordial black holes is defined by the PBH density and the factor so-called clustering parameter ζ. Also, we will consider that the radius of the cluster, is longer than the mean distance between primordial black holes $\tilde{x} \gg \bar{x}$. Hence, in this case, the expression for the mean distance given by (3.43) is given by

$$\bar{x_i} = \left(\frac{3M_i}{4\pi\rho_{eq} f\psi(M_i)\, dM_i\, \zeta} \right)^{1/3} . \tag{3.59}$$

It is straightforward to show that now the factor we have denoted as the mean distance between black holes with mass M_i and M_j is $\bar{x}_{ij}^3 = 3M_t/(8\pi\rho_{eq} f\zeta)$ and therefore, the value of the semi-major axis a corresponds to

$$a \approx 0.1 \left(\frac{3M_t}{8\pi\rho_{eq}} \right)^{1/3} \left(\frac{X}{f\zeta} \right)^{4/3} . \tag{3.60}$$

This modification of the semi-major axis a will cause the angular momentum to also depend on the value of the clustering parameter as follows

$$j = \left(\frac{85}{3} \frac{M_i M_j M_t f^4 \zeta^4 t}{(0.1\bar{x})^4 X^{16/3}} \right)^{1/7} . \tag{3.61}$$

It has also been shown in A.1.2 that the value of j_x is the same as in the previous cases and it can follow the same procedure. Therefore, the characteristic value of the dimensionless

separation parameter X_* is calculated in the same way as in the previous cases [4], except that we have to introduce the clustering parameter, obtaining as a result

$$X_* \approx 0.032\, M_t^{-1/37} \zeta^{16/37} f (f^2 + \sigma_{eq}^2)^{-21/74} (M_i M_j)^{3/37} \left(\frac{t}{t_0}\right)^{3/37} . \tag{3.62}$$

Using the values obtained in (3.56) and in (3.62) and following the same process as in (3.58), we get that the black hole merger rate considering a clustered distribution is

$$\begin{aligned} \frac{d\mathcal{R}(t)}{dM_i dM_j} \approx (3.7 \cdot 10^6)\, \zeta^{16/37} f^2 (f^2 + \sigma_{eq}^2)^{-21/74} (M_i + M_j)^{36/37} (M_i M_j)^{3/37} \\ \cdot \left(\frac{\psi(M_i)}{M_i} + \frac{\psi(M_j)}{M_j}\right) \min\left(\frac{\psi(\mathrm{M_i})}{\mathrm{M_i}}, \frac{\psi(\mathrm{M_j})}{\mathrm{M_j}}\right) \left(\frac{\mathrm{t}}{\mathrm{t_0}}\right)^{-34/37} , \end{aligned} \tag{3.63}$$

which is dependency of the clustering parameter is similar to the result of the article [27].

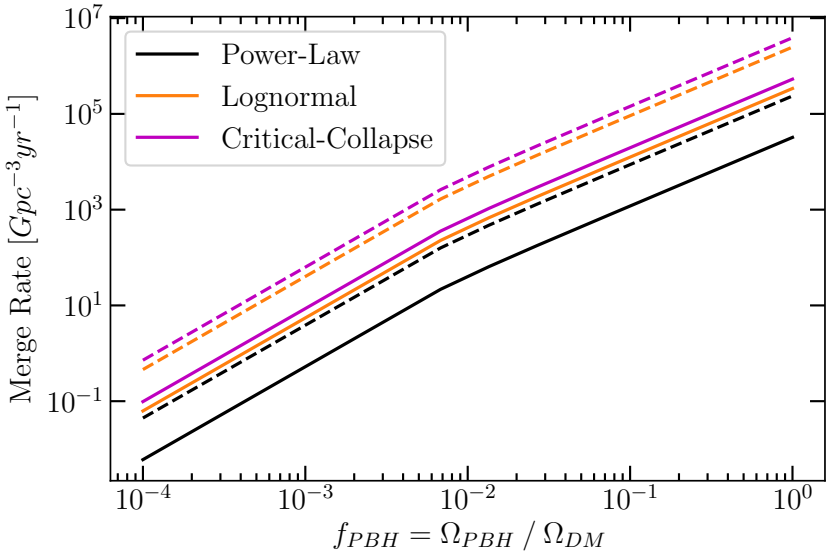

Figure 3.5: Comparison of the total merger rate per volume unit as function of the DM fraction of PBHs f_{PBH} at present time assuming clustered distribution approximation and uniform distribution. *Black solid line:* shows the merger rate for Power-Law mass function with parameters $\alpha = 2.2$ and $\delta = 20\,\mathrm{M}_\odot$. *Orange solid line:* the Log-Normal mass function with parameters $\sigma = 1$ and $M_c = 30\,\mathrm{M}_\odot$. *Magenta solid line:* the Critical Collapse mass function with the parameters $\beta = 2.85$ and $M_c = 30\,\mathrm{M}_\odot$. *Striped lines:* the same total merger rate except we will consider a clustering distribution with clustering parameter $\zeta = 100$

However, these implications are not entirely exact since as the clustering increases, other effects can arise that decrease the merger rate at present. One of these effects is

[4] Even though X_* depends on ζ, this parameter will not increase X enough so that the condition that $e^{-X} \approx 1$ is not fulfilled.

the disruption of the PBH binaries, due to their increased density. This effect is based on a third black hole approaching and staying close enough to disturb the binary system, causing a change in the angular momentum or distance between them. It depends on the effective cross-section of an encounter between PBHs that increases with the increasing density and is, therefore, larger when PBHs are distributed in clusters. Articles as [33] deal with this effect in the case of clustered spatial distribution. Nevertheless, as we deal with the clustered case in an approximate method, we are only concerned with this effect when taking a value for the clustering parameter.

We have decided to take some order-of-magnitude values of the clustering parameter to see the effects on the merger rate. For that reason, we have considered the values $\zeta \in \{1,\ 10,\ 100\}$. Despite these values are reasonable according to the article [31], this parameter depends heavily on the formation scenario that we have considered.

Chapter 4

Comparison with the merger rate by LIGO/Virgo

In this chapter, we will use the different merger rate models obtaining in chapter 3 to get the constraints on the primordial black holes abundance. For that, we will compare the experimental merger rate provided by the LIGO/Virgo detectors with the theoretical merger rate we have obtained in each model, searching for the maximum value of abundance for which both rates coincide. However, this is not straightforward when dealing with more realistic models such as an extended mass function since it does not depend only on the abundance value. Therefore, it is common to use a likelihood analysis, where we analyse which merger rate parameters best fit the LIGO/Virgo data. This analysis is beyond the limitations of this work. So, we will only analyse discrete characteristic parameters of the mass functions. Although this approach implies a loss of generality, it will reduce the number of parameters on which the merger rate depends. Thus, it will be possible to obtain the constraints on the PBH abundance. Once we get them, we will observe how they vary for different models and parameters and we will discuss them.

We will divide the chapter into three main parts. The first one will be an introduction of the data to be used, section 4.1, the second part we will compare the theoretical merger rate with Virgo/LIGO data, section 4.2 and the last part one the results obtained, section 4.3.

4.1. Introduction LIGO/Virgo data

LIGO and Virgo, as already mentioned, are two experiments capable of detecting gravitational waves located in the U.S.A and Italy respectively. For detecting these waves, they observe the interference of two lasers to measure whether the GW have modified the space of its length path. Nevertheless, gravitational waves are weak and can be affected by detector noise. It is, therefore, common to compare the measurements between the two detectors to rule out that the detection is coming from other sources.

The first confirmed gravitational wave event was detected by LIGO in 2015. Since then, the LIGO team has carried out three detection periods, named O_1, O_2 and O_3a, the

last one took place in 2019 and the measurements doubling in the latter period. After obtaining the measurements and checking for possible noise, the LIGO Scientific Collaboration and Virgo perform the analysis of the experimental data. For this, they use a maximum likelihood analysis using a selected data for a set of typical astrophysical black holes mass functions. With this analysis, they could obtain the parameters that best fit the data of each mass function.

Using these mass functions and the number of events observed, they also estimate the merger rate. Therefore, although an analysis of the theoretical models made in this work based entirely on the LIGO/Virgo data is rather complicated, we can use the results delivered in their last published article. In particular, we will use the differential merger rate assuming a 'Power-Law + Peak' mass function to compare since it is the best fit to the experimental data. This differential rate can be seen in the Figure 4.1.

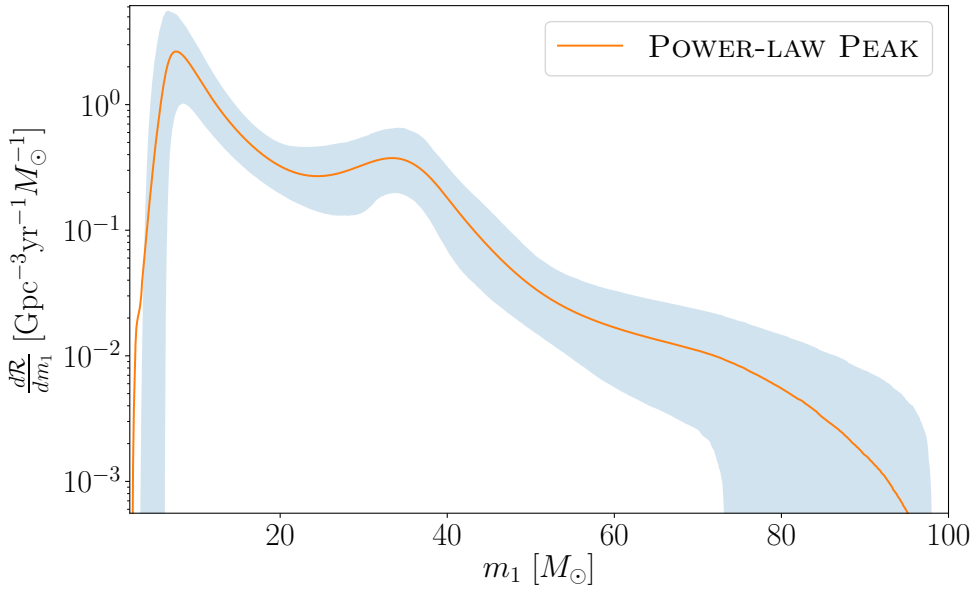

Figure 4.1: Plot extracted from the article [28], where it is shown the differential merger rate in function of one of the black hole mass M_1. *Solid line:* the mean value of the differential merger rate. *Shaded:* the $R_{90\%}$ credible region.

However, such analyses cannot distinguish between primordial and astrophysical black holes. Therefore, the merger rate obtained corresponds to primordial and astrophysics black holes. It is also important to note that the detectors are limited to a certain precision in their measurements. So if the gravitational waves are not 'strong' enough, they are not detectable. This in turn places a limit on the measurement of black hole masses since the mass is directly related to the amplitude of the GW. We could see in Figure 4.1, where there is a low-mass cut-off.

It is noteworthy that these restrictions obtained from GW are not the only ones since there are other effects as mentioned above. In some cases, we have to take into account these restrictions due to other effects as explained in the introduction 1.

4.2. Comparison of obtained merger rates

One of the objectives of this work is to obtain the maximum black hole abundance for each model described in the previous chapter. To do so, we will compare the differential merger rate obtained with these models with that of the LIGO/Virgo analysis as discussed in the previous section. However, as the merger rate depends on the mass functions, which in turn depend on two parameters (except for the monochromatic case), a full analysis of all the cases is out of the scope of this work. We will consider instead only a few discrete values of each main parameter of each mass function. These values should be sufficiently different to cover the most interesting range of parameters. In addition, we will always try to ensure that these functions are not too wide to exceeds the mass range $[10^{-1}, 10^{3}]$ $M_\odot$ since they would be restricted by other effects such as dynamic effects.

The values that have been selected for each parameter are as shown in Figure 4.2. Once we have fixed one of the parameters of the mass function, we will calculate for each value of the remaining parameter the maximum black hole abundance.

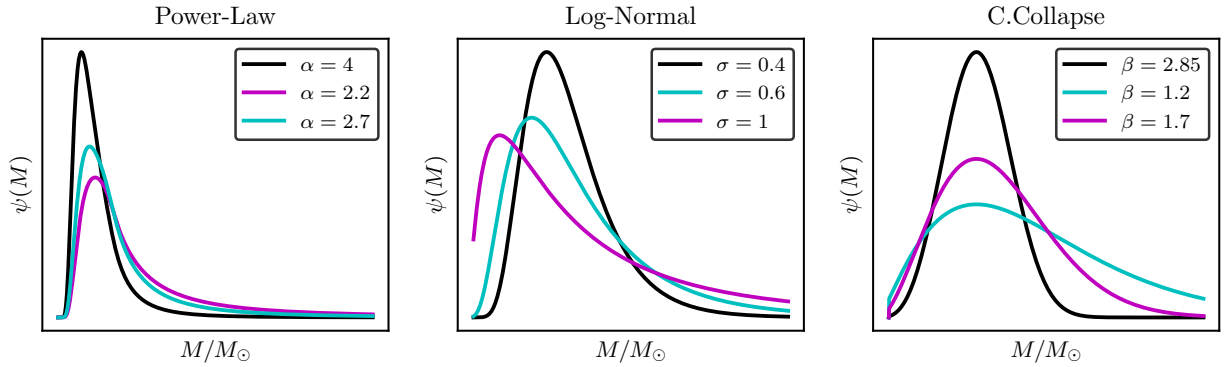

Figure 4.2: It shows the mass functions to be used in the analysis. It is important to note that these functions also vary with the parameters M_c in the case of Log-Normal and Critical collapse and δ in the Power law mass function.

For this purpose, we obtain $d\mathcal{R}/dM_1dM_2$ using the equation 3.58 we developed in the previous chapter. This function will be integrated for the value M_2 in the mass range [3,100] $M_\odot$, resulting in the function $d\mathcal{R}/dM_1$. Finally, we will compare this $d\mathcal{R}/dM_1$ function until we find which value of the PBH abundance intersects the upper limit of the confidence interval given by LIGO/Virgo. This comparison is made in the interval [6, 85] $M_\odot$ since, as mentioned above, for small masses LIGO and Virgo lose sensitivity and the upper limit is influenced by other effects. Through this comparison, we will estimate the maximum value of the abundance of primordial black holes.

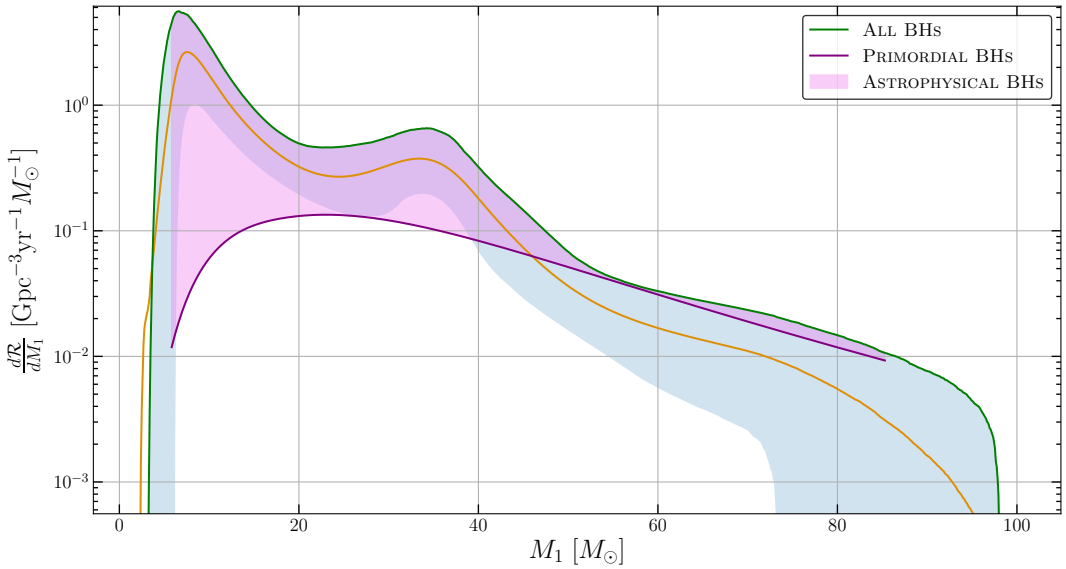

Figure 4.3: It shows an example of a comparison between the differential primordial black hole merger rate and the differential merger rate inferred by LIGO/Virgo. This example is the case where a lognormal mass function with $\sigma = 0.6$ and $M_c = 38\,\mathrm{M}_\odot$ has been considered, observing that they intersect when the value of abundance is $f_{\mathrm{PBH}} \approx 8 \cdot 10^{-4}$. This intersection occurs around $M_1 \sim 57\,\mathrm{M}_\odot$.

The function $d\mathcal{R}/dM_1$ given by our model intersects with the upper bound at only one value of M_1. In this comparison, we are not seeking to fit our model to the upper limit since we have to remember that this upper limit given by LIGO/Virgo includes both possible primordial black holes and astrophysical black holes. So the difference in the rest of the function can be considered the influence of astrophysical black holes on the differential collapse rate. It can be seen in Figure 4.3.

This method will thus be useful to get the constraints for each of the mass functions, as well as for the clustering approach or the 'monochromatic' case [1]. Nevertheless, the comparison in this last case presents some problems since it is a narrow mass function and therefore, it is not possible to obtain the constraints for masses lower than 6 $\mathrm{M}_\odot$ and masses larger than 85 $\mathrm{M}_\odot$.[2] Therefore, we will no longer compare the differential merger rate but the total merger rate of the primordial black holes for the range masses [0.1, 2] $\mathrm{M}_\odot$ and [100, 400] $\mathrm{M}_\odot$. In this way, we could consider the upper limit of the total merger rate credible region obtained in the experimental analysis and compare it with the one obtained with the equation (3.42). It will allow us to obtain the constraints in most of the PBH mass range. This upper limit will be taken from the article [34] and their recent update [35] in the mass range [0.1, 2] $\mathrm{M}_\odot$. We have decided to take both in order to observe their differences since the first one is an analysis of the first two O_1 and

[1] Monochromatic constraints can not be obtained with this method. However, we will use a Log-Normal mass function with a low standard deviation that we consider as monochromatic.

[2] It should be noted that if we consider such a mass function and we take a value of Mc outside the comparison range, as the value of $d\mathcal{R}/dM_1$ is not extended, it will not fall within the comparison mass interval.

O_2 detection and the second one includes the O_3a data. The last one has been published recently [35]. So we can update the PBH abundance constraint. For masses larger than 85 $M_\odot$, we will use the upper limit $R_{90\%}$ from [36] where they perform an analysis of the PBH merger rate and consider only the O_1 and O_2 measurements.

Despite this, there will still be a small gap between constraints where it is not possible to derive the constraints using these comparison methods. In this range, an interpolation can be performed using the constraints given by both comparison methods. This interpolation is only for visual purposes. Nevertheless, our comparison method is valid for any analysis where the upper limit of the confidence region of the experimental merger rate is obtained. It allows us to update the constraints as more recent LIGO/Virgo data or other future experiments are published.

4.3. Constraints in the abundance of PBHs

The constraints on the abundance of primordial black holes provide us with information about this dark matter candidate since they allow us to distinguish which masses of primordial black holes would be most probable and at what is their abundance. As more and more events are obtained in the LIGO/Virgo detectors, these constraints will be updated and we will hence be able to determine, together with the others constraints given by other effects, what approximate fraction of matter is constituted by PBHs in our Universe. It is also worth noting how it varies according to which initial conditions as the mass function and to observe their importance in the merger rate calculation.

Using the method explained in the previous section, we will obtain the maximum abundance of black holes for the monochromatic case in section 4.3.1, for the case of an extended mass function considering the parameters given in 4.2, in section 4.3.2. We have also added the clustering factor to observe how the constraints change in section 4.3.3 and finally, we will compare some of our results with those given in article [37] where they have performed a different calculation, in section 4.3.4.

4.3.1. PBHs constraints assuming a monochromatic mass function

As discussed above, to obtain the constraints in the monochromatic case, we have to perform at least two kinds of comparisons. One for masses smaller than 2 $M_\odot$ and larger than 85 $M_\odot$ and another one for masses between 6 $M_\odot$ to 85 $M_\odot$. We can use this method only if an extended mass function is considered. So, we have to approximate the Dirac delta to a Log-Normal mass function with a very small sigma of $\sigma = 0.05$. Although we can make a similar approximation for the other mass functions, this is the simplest case. This approximation will provide a modest error in our calculation. However, we will perform a rough estimate of the maximum abundance of PBH in that interval.

These methods allow us to obtain values in the intervals [0.1, 2] $M_\odot$, [6, 85] $M_\odot$ and [100, 400] $M_\odot$, covering a large portion of the range of masses between [0.1, 10^3] $M_\odot$. Hence, we will also show the constraints if we extrapolate between the two intervals. The result is shown in the Figure 4.4.

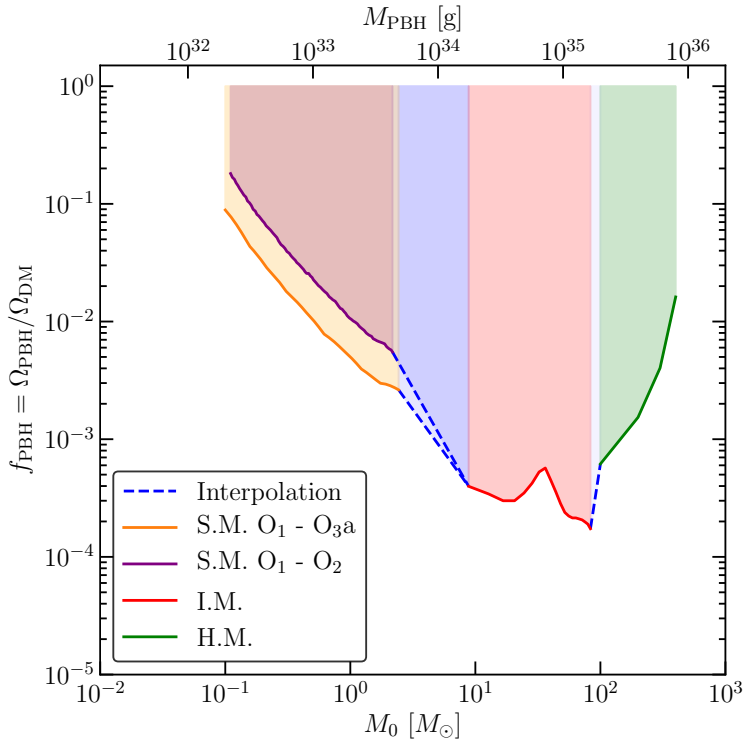

Figure 4.4: Constraints on the fraction of DM that PBH constitute , f_{PBH} assuming monochromatic mass function. *Blue:* corresponds to the interpolation between constraints. *Red:* results obtained by comparison with [28] for a intermediate mass (I.M.) PBHs . *Purple:* results obtained considering [34] for Sub-solar masses (S.M.). *Orange:* results obtained using the comparison with updated with [35], where they add the O_3a data. *Green:* results achieved comparing with [36] for high masses (H.M).

In addition, several properties can be observed in these constraints. The first one is that we will see that the comparison made with article [34] is more stronger when the O_3a data is added. This difference could be since no merging of subsolar-mass binary primordial holes has been observed so far in any data collection. It implies that, despite increasing the exposure time, it has not yet been possible to measure PBHs in O_3a.

Another property that is also related to this effect is the mass peak around $M_{\rm PBH} \sim 30 M_\odot$. This peak could be explained by the fact that LIGO and Virgo have high precision in that mass range, and the data are slightly biased. As we have used these data to derive the constraints, they are also influenced. Since we have considered that some of these observations are caused by primordial black holes, these constraints become weaker as there are more events. For this reason, a noticeable peak in the function.

On the other hand, we will observe that the constraints obtained for large mass do not form a 'continuous' shape with the result of intermediate masses. We can note that the constraints of the method used for large masses are weaker. This is probably due to the fact that [36] only used data obtained from O_1 and O_2 and in [28] the data of O_3a is also considered. So, as with the low mass constraints, the effect of adding O_3a will make the constraints stronger.

It can also be concluded that the fraction of DM that PBHs constitute for the range of masses 1-10 $M_\odot$ is roughly estimated to be $f_{\mathrm{PBH}} \approx 5 \cdot 10^{-3}$ and for the range 10-100 $M_\odot$ corresponds to $f_{\mathrm{PBH}} \approx 5 \cdot 10^{-4}$ in a approximately way. Also, we will consider that the constraint obtained for a monochromatic mass function is the one shown in the figure 4.5. The constraints obtained with the most recent article [35] have been considered as valid and the gaps have been fitted by interpolation.

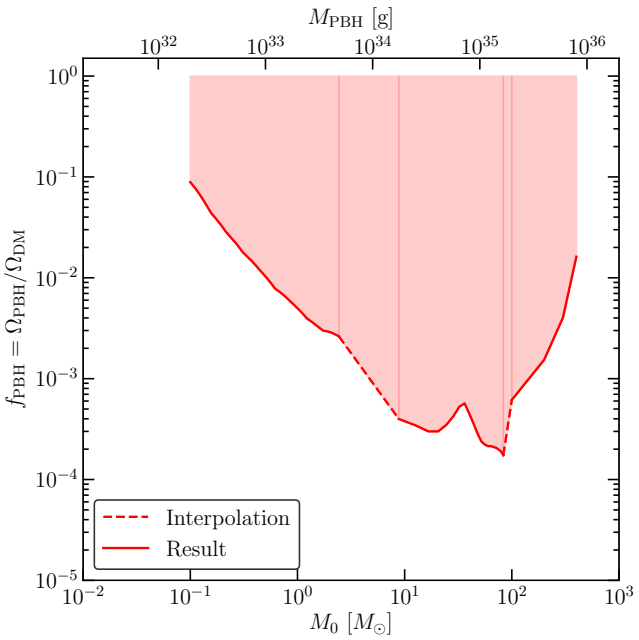

Figure 4.5: Total constraints on the fraction of DM that PBH constitute, f_{PBH} assuming monochromatic mass function. It is the same result as we have shown in Figure 4.5, except for the fact that we have collected them together.

4.3.2. PBHs constraints assuming an extended mass function

In this subsection, we will assume that the primordial black holes have an extended mass function. This assumption implies that the method explained in section 4.2 for obtaining the constraints is valid over the whole interval. On the other hand, we have to consider the limited scope of the work. Hence, we have only obtained the constraints for the cases shown in Figure 4.2. This procedure would be valid for any value of these parameters that we have set, as long as they fall within a reasonable interval. We will select the parameters to encompass the major number of cases and for the interest to the

comparison with other articles' results. These restrictions are shown in Figure 4.6 where it is possible to observe the difference both between the same function when varying the main parameter $\{\sigma, \beta, \alpha\}$ and between different mass functions.

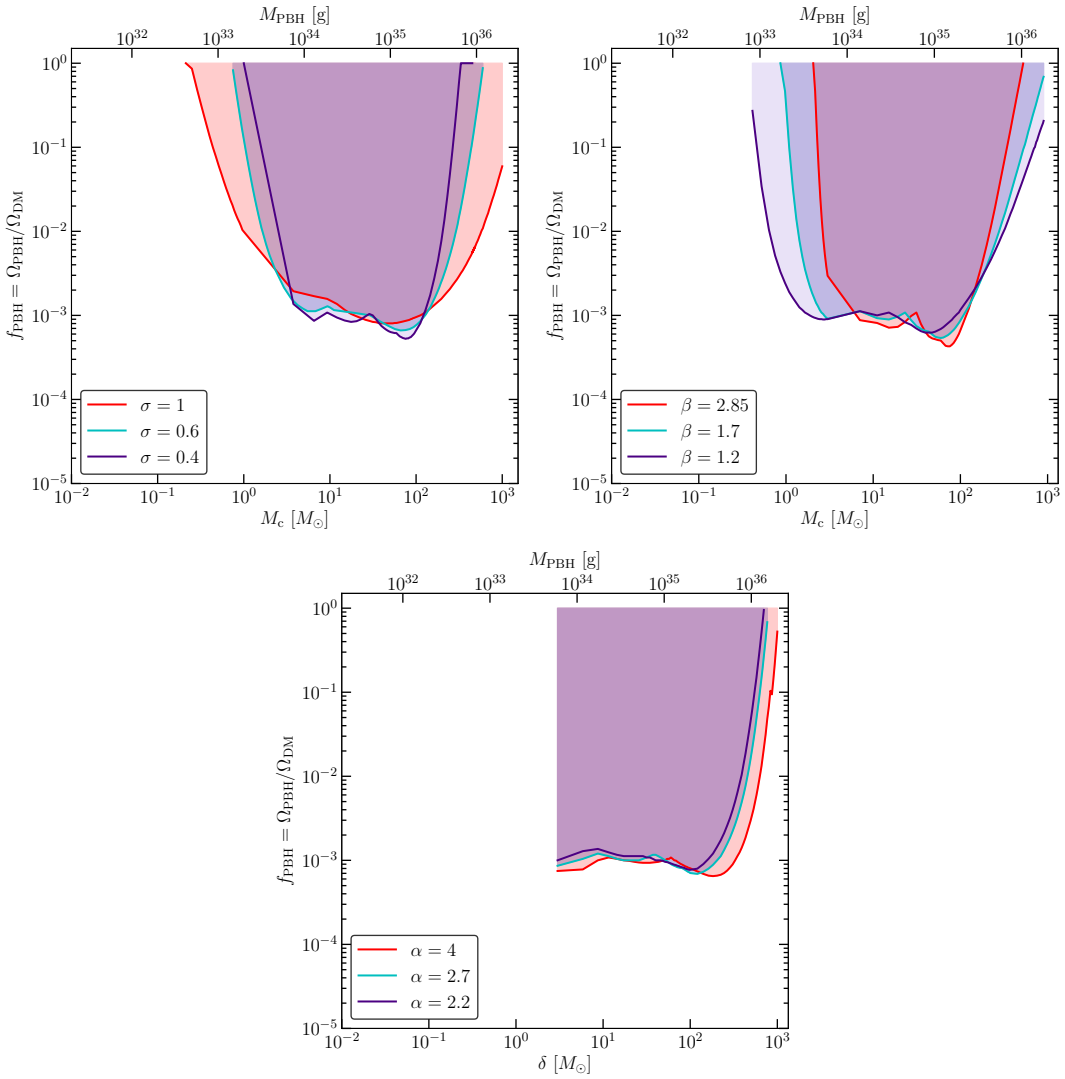

Figure 4.6: Constrains on the fraction of DM that PBH constitute , $f_{\rm PBH}$ assuming extended mass function. *Top left*: constraints for the case a Log-Normal mass function. *Top Right*: constraints for the case of Critical Collapse mass function. *Bottom centre*: constraints for a Power-Law mass function.

Some common properties can be observed in all mass functions. One of the most trivial to note is that if we assume a wide mass function, we will obtain a wider constraint that expands over a huger range of masses. For this reason, We have discussed above that such a function with a large $\sigma > 1$ and $\alpha > 5$ or low $\beta < 1$ would not be entirely appropriate, as we would have to take into account the constraints of other effects (Dynamical, Accretion, etc) as we could see in Figure 1.1. However, if we increase or decrease these values sufficiently, and the mass function becomes very narrow, the value of the constraints abundance would be weak for many of the mass range, in some cases allowing

us to come close to constituting all the dark matter. For instance, if we consider a high value of β, the range of mass [1, 10] $M_\odot$ and [200, 1000] $M_\odot$ we could have a maximum abundance equal to one.

Another of the common properties is that the maximum abundance for a 10-100 $M_\odot$ PBH masses are lower than the other range of mass. This means that for this mass range a much larger number of detected events would be expected. Also, this is affected by considering whether or not the measured black holes are primordial, as in the case of the monochromatic case. In fact, it can be observed that for the mass range 30-40 $M_\odot$ the peak is maintained, although much less noticeable. So we can conclude that for masses between [10, 100] $M_\odot$ in neither case will it be possible to obtain that the primordial black holes constitute all the dark matter, on the basis of the observations so far. It can even be approximated for that range of masses that for any sufficiently narrow mass function the constraints will be around the value of $f_{\rm PBH} \approx 10^{-3}$ which is still weaker than if we consider a monochromatic mass function as seen in the previous subsection.

There are also differences when considering different mass functions, such as how the abundance value increases for small masses. It is easy to see that for the Log-Normal case, the constraints tend to extend more while the Critical Collapse mass functions have a much sharper cut-off, especially when considering a Power-Law type function. This mass function considers a minimum mass of primordial black holes, in this case, has been considered to be the most common value corresponding to 3 $M_\odot$ and hence, this is reflected in the constraints. The other clear difference between the Power -Law mass function and the other functions is that the variation of the parameter α does not affect the restrictions too much since it only extends them a little more to higher mass ranges. However, for the Log-Normal and the Critical Collapse mass function, we could see that by decreasing or increasing the parameter, the constraints change.

4.3.3. PBHs constraints assuming clustering and an extended mass function

In this subsection, we will consider that merger rate is given by (3.63) instead of (3.58) i.e. we will include the clustered spatial distribution case with an extended mass function. This case implies a change in the constraints on the abundance of primordial black holes. There are many possible values of the clustering parameter and mass function parameter to be analysed. Nevertheless, as the objective is only to observe the effect, we will compare it with a clustering effect in orders of magnitude $\zeta \in \{1, 10, 100\}$ with the most representative parameter values for each mass function. It has accordingly been considered for the Log-Normal mass function a characteristic parameter $\sigma = 0.6$, for the Power-Law $\alpha = 4$ and for Critical Collapse $\beta = 2.85$. The approximate constraints are shown in Figure 4.7.

To estimate the effect of clustering, we will consider that there exists an excess probability of locating a black hole in a given volume. This excess has been considered constant over a certain distance of the cluster, obtaining the result of (3.58), where only a constant

parameter in the differential merger rate is added. Since this factor does not influence the shape, we will expect that they have the same shape.

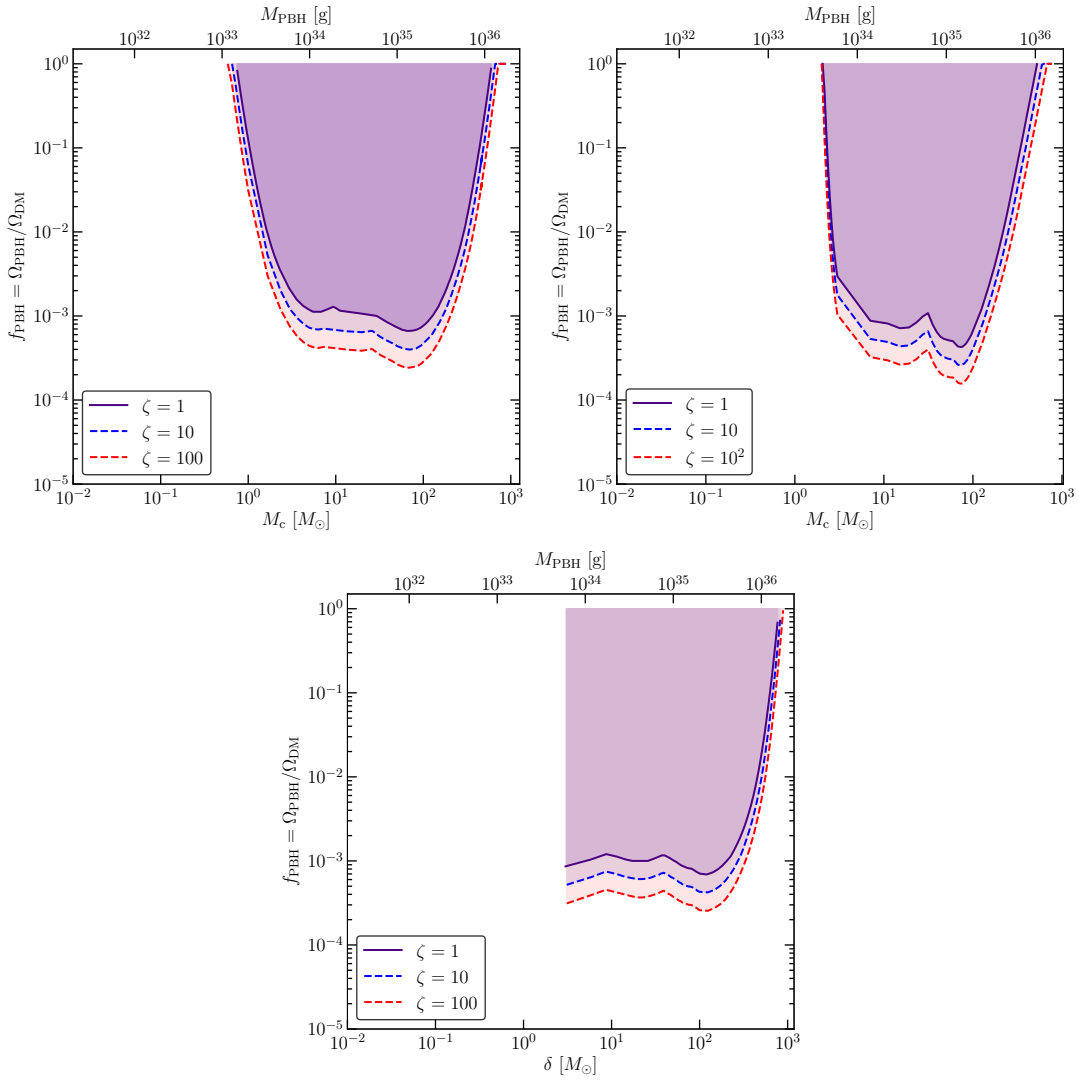

Figure 4.7: Constraints of the fraction of DM that PBH constitute , $f_{\rm PBH}$ assuming extended mass function and clustered spatial distribution. *Top left*: constraints for a Log-Normal mass function. *Top Right*: constraints for the Critical Collapse mass function. *Bottom centre*: constraints for a Power-Law mass function.

However, if we consider a higher clustering parameter, the value of the merger rate increases as there is a higher probability of binary formation. This increase in the expected merger rate causes the constraints to be stronger, as can be seen in Figure 4.7. In addition, we will observe the discrepancy of the constraints when considering different clustering parameters. We have also estimated that the fraction of the abundance of primordial black holes decreases $\Delta f_{\rm PBH} \approx 5 \sim 10^{-4}$ when consider a clustering parameter $\zeta = 100$.

The impact of clustering into the PBHs abundance constraints is small, from the

point of view of the approximation made in this work. We can hence consider that the constraints without clustering can encompass the clustering case if we account for possible errors in the comparison methods.

4.3.4. Constraints comparison

We will compare the results with the results obtained in the article [37] to analyse the differences and similarities. In this article, the calculation is only performed for the monochromatic case and the case of a Log-Normal mass function with $\sigma = 0.6$, so the comparison will only be made with those results, which have already been shown in the previous subsections. This comparison can be seen in Figure 4.8. We will observe that there are discrepancies between the two models. However, both the shape and the approximate magnitude range of both are in agreement. It can be assured that our approximation method has given results in agreement with the expected ones.

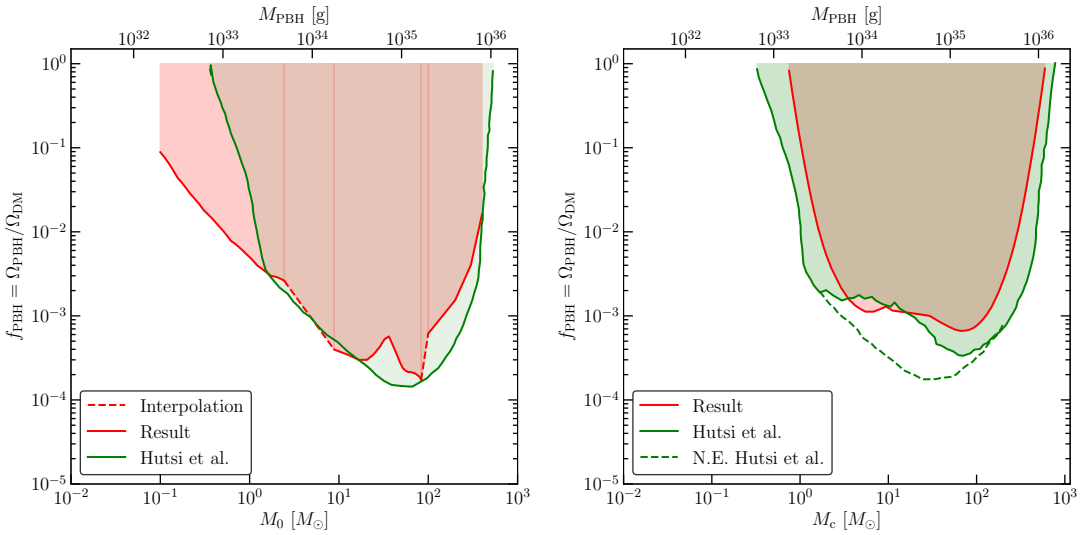

Figure 4.8: Comparison between the PBH abundance constraints obtained in this work and the obtained in [37]. *Left*: comparison when we assume monochromatic mass function. *Right*: comparison when we assume Log-Normal mass function with $\sigma = 0.6$. The dashed green line indicates the result obtained by [37] when considering that none of the observed events have been originated by PBHs (N.E.).

Let us now analyse the possible causes of this discrepancies. Looking at the plot on the left, i.e. the comparison when a monochromatic mass function is assumed, quite a few discrepancies can be observed. It can be seen that for masses in [6, 85] $M_\odot$ the constraints proposed by the article are stronger than those obtained in this work. The reason for this is that the article [37] assumes that all black holes observed in LIGO/Virgo are astrophysical. As we have discussed above, this assumption places much more severe constraints on the merger rate, since a lower abundance of primordial black holes is required for the merger rate to coincide with no observation at all. This difference is observable when comparing both plots, including the peak discussed in the previous subsection.

Moreover, we are interpolating between mass intervals, so our plots in the region of interpolation must be considered merely as an educated guess. Nevertheless, the maximum discrepancy is observed for sub-solar mass values. A possible explanation for this discrepancy is the consideration of binary disruption and other merger rate suppression factors like the collision between PBHs. These factors increase in strength when f_{PBH} is larger since the number of PBHs increase these effects has a major probability to occur. Therefore, if they consider these suppression factors, the expected merger rate decreases and makes the constraints weaker, especially at the extremes. For the case of large masses, a similar situation occurs, although it cannot be observed since these constraints only extend up to 400 $M_\odot$. If we extrapolate, we notice that these constraints proposed in the article also decrease more rapidly than those obtained in this work, which confirms the possibility that this is due to the suppression factor. Finally, it is noteworthy that the data selection does not have to be the same. In fact, in a high mass, we have considered O_2 run, and the article takes the data for O_3a.

The situation is different for the comparison of the constraints assuming a Log-Normal mass function. In [37], they realized two different analysis for the Log-Normal mass function. One in which it is considered that none of the events detected in O_3a are primordial black holes, shown in dashed lines and other analysis in which they consider that all merger detected is PBH. Also, they assume that the intermediate zone between both restrictions is when part of the observed events are primordial and the rest are astrophysical. This region is where the function obtained in this work should be. Nevertheless, in general, the constraints obtained are weaker. The reason for the discrepancy could be the selection of the LIGO/Virgo data and the method used.

To sum up, we have developed a simpler method than the careful likelihood analysis, and we have obtained results in line with them. Hence, this method can be used for observing the properties of the constraints assuming different initial conditions.

4.4. Current constraints scenario

Finally, in this last section, we will show the monochromatic and the Log-Normal functions, together with other effects. We will choose them since they are the most common. In this way, we can observe the current scenario of the total constraints on the abundance of primordial black holes[3]. In these figures, it is seen that although at high masses there are already other types of constraints that limit the abundance of primordial black holes. Nevertheless, in the mass range [1, 100] $M_\odot$ these constraints set the abundance. We have changed the GW constraints of Figure 1.1 to the results obtained in the previous sections.

[3]The data for the rest of the constraints have been obtained from `https://github.com/bradkav/PBHbounds/`

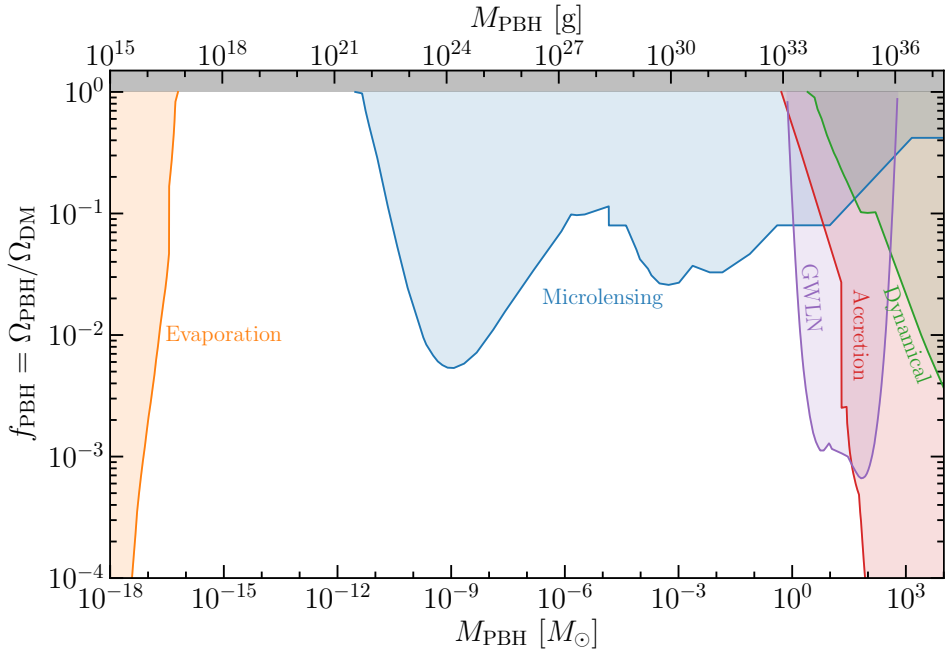

Figure 4.9: All constraints on the PBH abundance, $f_{\rm PBH}$, with mass $M_{\rm PBH}$. They coming from PBH evaporation, microlensing, PBH accretion, dynamical constraints and the constraints obtained in this work, for a Log-Normal mass function ($\sigma = 0.6$) by GWs.[4]
.

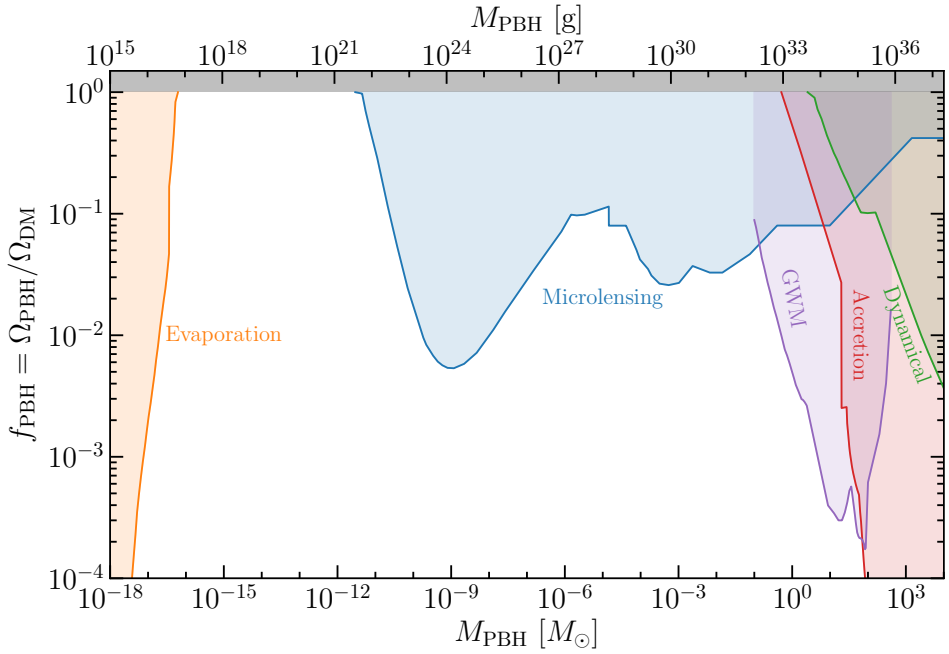

Figure 4.10: All constraints on the PBH abundance, $f_{\rm PBH}$, with mass $M_{\rm PBH}$. They coming from PBH evaporation, microlensing, PBH accretion, dynamical constraints and the constraints obtained in this work, for a monochromatic mass function by GWs.[5]

We could observe that the only mass range in which primordial black holes can constitute all the dark matter is $[10^{18}, 10^{21}]$ g, a range of masses similar to the asteroid mass. The reason for this is not that there are no constraints in that mass range but that the experiments are not yet sensitive enough to detect these PBHs. Even so, there is still much work to be done before we can conclude that black holes are now a part of dark matter. It is expected that improvements in both the theoretical developments of the evolution and formation of primordial black holes such as those discussed in this work and the experimental developments by extending the range and precision of experiments will determine the complete PBH constraints.

[5]The data for the remaining constraints have been obtained from `https://github.com/bradkav/PBHbounds/`

Chapter 5

Conclusions and future work

Primordial black holes have become one of the most popular dark matter candidates in recent years due to the wide range of masses they could have and since experiments can now detect their effects. Hence, if one establishes a background theory of such effects and compares it with the measurements that are being obtained by current experiments, it is possible to get constraints on the fraction of dark matter they constitute. These effects are, among others, the microlensing effect, evaporation, accretion effect and gravitational wave emission.

In this work, we have obtained constraints on the abundance of primordial black holes using the most recent gravitational wave measurements from the LIGO and Virgo experiments. Furthermore, it has been analysed how these constraints behave when considering different assumptions such as a clustering distribution or an extensive mass function, which is more realistic. This process is not straightforward, so some of approaches have been considered and discussed throughout the work.

We have had a brief discussion on what could cause the formation of primordial black holes. In this discussion, we have focused on the most simple formation process, which is the collapse of large density perturbations in the radiation-dominated era. We have also noted that, even if we are considering the most simple formation process, the current knowledge about the properties and initial formation conditions of primordial black holes is scarce. Therefore, we have to include as many scenarios as possible, assuming different initial assumptions.

A review of the evolution of PBHs was also done, focusing on the case of binary systems. The number of these binary systems formed in the early universe depends on the abundance of PBHs and their clustering properties since they require to be close enough in the early Universe for the gravitational force to overcome other forces such as the Universe expansion. Once the PBH binaries are formed, they will generate gravitational waves as they orbit, losing energy in the process. We have derived in this work the calculation of the time required for this kind of binary system to merge, considering the emission of gravitational waves. Finally, we have explained that an inspiral gravitational wave is created in the merger of these systems, which can be detected on Earth by experiments such as LIGO and Virgo. These detections allow us to obtain the experimental merger

rate by analysing these GW.

The basis of this work is the theoretical development shown in chapter 3. In the preliminary sections, we have shown the implications of assuming different conditions such as the clustering effect or the extensive mass functions. Afterwards, the theoretical development to obtain the merger rate of the simplest case, i.e. the monochromatic one, has realised and then generalised. As a result, the different merger rates for each model have been obtained.

Moreover, the different theoretical models proposed and the most recent analyses published by LIGO/Virgo have been used to obtain the constraints on the abundance of primordial black holes. We have decided to perform a basic comparison since a more rigorous analysis was beyond the time constraints of the work. Nevertheless, we have got that the discrepancy with the analysis performed in the article [37] is not very significant.

To sum up, we have obtained that the maximum abundance for primordial black holes in a range of masses [6, 90] $M_\odot$ is $f_{\rm PBH} \approx 10^{-3}$ assuming an extensive mass function. This abundance value decreases by one order of magnitude in the case of a monochromatic mass function, i.e. $f_{\rm PBH} \approx 10^{-4}$. Finally, in the clustering approach, if a high clustering parameter is considered $\zeta = 10^2$ the constraints become tighter, reaching maximum abundance values of $f_{\rm PBH} \approx 10^{-5}$. This analysis suggests that primordial black holes in this mass range constitute only a small fraction of the dark matter. Nonetheless, this fraction may be significant enough to affect some cosmological phenomena that are currently under study.[38] Consequently, the study of these dark matter candidates is far from closed.

Although our calculations have been done in a detailed way, it has not been possible to explore all the concepts and effects that can occur in the dynamics of primordial black holes due to the limited scope and time scale of this work. Some of these future works could be:

- Firstly, a future work that could be done would be to obtain the constraints by performing a likelihood analysis. This kind of analysis searches for the parameters of the merger rate that best fit the selected data from the LIGO/Virgo experiments. This analysis is more rigorous than the one done in this work. It includes the possible detector bias, the maximum measured redshift and among other factors. Therefore, it would be of great interest to start from the theoretical results obtained here and observe the form of the constraints and if they fit the PBHs constraints given by the approximation. Additionally, more complex mass functions such as Multi-peak or broken Power-law can be considered using this procedure for fitting both primordial black holes and astrophysical black holes simultaneously.
- It is not still known whether the initial spatial distribution of the black holes is uniform or clustered. It is convenient to consider both cases in detail. However, we have not done a complete theoretical development of the clustering effects since it was beyond the scope of the work. For that, we have approximated the two-point correlation function to be constant over a certain distance, but in reality

this approximation may not be fulfilled. Hence, a careful study should contain more information on what happens if the correlation function depends on the PBHs distance in different ways.

- A further area of great interest in the theory of primordial black holes is the knowledge of their formation. As discussed in this work, there are many ways in which these massive objects can be formed, and studies have been done on which type of formation causes which mass function. For instance, a topical case is the formation of primordial black holes by pressure decay in the QCD transition, as the pressure prevents the collapse of PBHs. This scenario of formation results in a Multi-Peak mass function with determined parameters. Using an analysis similar to the one discussed in this work would make it possible to obtain better constraints if we consider this scenario.

- Finally, another future work is to consider more possible effects that could occur during the evolution of primordial black holes and to study the variation of the PBHs constraints. Some of these effects have already been mentioned in this work, such as the disruption of binaries or the creation of PBH binaries at the present time. Nevertheless, they have not been discussed in detail. Disruption considers the probability that a third very close black hole will perturb the characteristics of the binary system. [33] On the other hand, if two black holes are close enough at present they could result in a binary system that would collapse and contribute to the merger rate.[39] Also, there are more possible effects that have not been mentioned, such as the possibility that the remaining dark matter influences the merger rate, the so-called "dark dress" effect, or the accretion of baryons in their evolution.[40] All these effects complicate the calculation of the merger rate but make the model more realistic and contribute to the development of black hole dynamics.

This work allowed me to develop my knowledge about branches such as Cosmology and Astrophysics. In addition, I have been able to contribute to the primordial black holes theory with our approximation for the case of clustered spatial distribution and with the development of a simple method to obtain the abundance constraints assuming different mass functions. Finally, I would like to emphasise that I had learned a lot about software programming and of course, about English to be able to elaborate this work.

We can conclude that this work can be used as an estimation of the fraction of dark matter that constitutes primordial black holes for different simple cases in an approximate range of mass [1, 100] $M_{\odot}$. Moreover, we have used the most recent LIGO/Virgo analysis to update these constraints. This work is a basis for future works on this dark matter candidate. We have therefore achieved the objective of providing some light on this problem in physics at present.

Appendix A

The reduced angular momentum probability distribution

In this appendix, we will obtain the probability distribution of the reduced angular momentum giving by the rest of the PBHs. Firstly, we will obtain it assuming a monochromatic mass function and then, we will generalise it to the rest of the models. The solution obtained in this appendix will be used to develop the theoretical models of chapter 3.

A.1. Reduced angular momentum by other PBHs

As we have discussed in section 3.2.3, the reduced angular momentum by all the PBHs is given by the equation (3.28), which corresponds to the super-positions of many variables that depend on some probability laws. These dependencies imply that the probability that the value of angular momentum lies between j and $j + dj$ is complicated to obtain. Therefore, one of the most common methods for solving this type of probability distribution problems is Markoff's method, whose solution is given by

$$W_N(\phi) = \frac{1}{(2\pi)^n} \int .. \int e^{i\rho\phi_0} A_N(\rho) d\rho^n \tag{A.1}$$

$$\tag{A.2}$$

$$\text{with} \quad \mathrm{A_N}(\rho) \equiv \prod_{\mathrm{k=1}}^{\mathrm{N}} \int \mathrm{e}^{-\mathrm{i}\rho\phi} \tau(\mathrm{q}) \mathrm{dq_k} \,, \tag{A.3}$$

where W_N is the probability distribution, ϕ represents the property to be studied, N is the number of variables that we will consider, τ is the probability of a giving coordinate q and ϕ_0 is a preassigned value of ϕ.[41]

To obtain the reduced angular momentum probability distribution by Markoff's method, we will assume that the PHBs are uniformly distributed in a spherical volume V. Also, we will consider that the volume and the number of PBHs N tend to infinity simultaneously in a way that the density $n = N/V$ is always constant. As j is perpendicular to $\hat{x}$, we only have to consider two dimensions. Therefore, using (3.28) equation, the probability

distribution is given by

$$W_N(j) = \frac{dP}{dj^2} = \lim_{V\to\infty} \frac{1}{(2\pi)^2} \int \exp\left(\mathrm{i}\rho\cdot\mathbf{j}\right) \mathrm{A_N}(\rho)\mathrm{d}\rho^2 \,, \tag{A.4}$$

where

$$\begin{aligned} A_N = \prod_{k=1}^{N} \int_V \exp\left(-1.5\mathrm{i}\sum_{\mathrm{p}=1}^{\mathrm{N}} \frac{\mathrm{x}^3}{\mathrm{y}_\mathrm{p}^5} \mathrm{y}_{\mathrm{p}\parallel}\mathbf{y}_{\mathbf{p}\perp}\right) \frac{\mathrm{dy_k^3}}{\mathrm{V}} = \left[\int_{\mathrm{V}} \exp\left(-1.5\mathrm{i}\frac{\mathrm{x}^3}{\mathrm{y}^5}\mathrm{y}_\parallel \mathbf{y}_\perp\right) \frac{\mathrm{dy}^3}{\mathrm{V}}\right]^{\mathrm{N}} \\ = \left\{1 - \frac{1}{V}\int_V \left[1 - \exp\left(-1.5\mathrm{i}\frac{\mathrm{x}^3}{\mathrm{y}^5}\mathrm{y}_\parallel\, \rho\cdot\mathbf{y}_\perp\right)\right] dy^3\right\}^{nV} = (1 - \jmath/V)^{nV} \,, \end{aligned} \tag{A.5}$$

with

$$\jmath \equiv \int \left[1 - \exp\left(-1.5\mathrm{i}\frac{\mathrm{x}^3}{\mathrm{y}^5}\mathrm{y}_\parallel\, \rho\cdot\mathbf{y}_\perp\right)\right] dy^3 \,. \tag{A.6}$$

Therefore, if we apply the limit, the result is given by

$$\lim_{V\to\infty} A_N = \lim_{V\to\infty} (1 - \jmath/V)^{nV} = e^{-n\jmath} \,. \tag{A.7}$$

We now can simplify $\jmath$, rotating the component $\mathbf{y}_{\mathbf{q}\perp}$ as $(\mathbf{y}\cdot\hat{x})\hat{x} + \hat{x}\times\mathbf{y}$ and we will use the variable change $v = (1.5\rho x^3\mathbf{y}^3)^{-1}$, so we will rewrite the equation (A.6) as

$$\begin{aligned} \jmath = 2\pi\rho x^3 \int_0^\infty \frac{dv}{v^2}\frac{d^2\hat{y}}{4\pi}\left[1 - \exp\left(\mathrm{iv}(\hat{\mathrm{y}}\cdot\hat{\mathrm{x}})(\hat{\mathrm{y}}\cdot\hat{\rho})\right)\right] = \\ 2\pi\rho x^3 \int_0^\infty \frac{dv}{v^2}\int_0^{2\pi}\frac{d\phi}{2\pi}\int_0^1 d\mu \left[1 - \exp\left(\frac{\mathrm{iv}}{2}\sin(2\phi)(1-\mu^2)\right)\right] \,, \end{aligned} \tag{A.8}$$

where we have changed the variables to

$$\hat{y} = \sin(\theta) \quad \hat{x} = \cos(\phi) \quad \hat{\rho} = \sin(\phi) \quad \text{and} \quad \mu = \cos(\theta) \,.$$

The integral of the exponential on (A.8) corresponds to the zero-order Bessel function $J_0(v(1-\mu^2))$. We will also simplify it more, by making another variable change as $u = v(1-\mu^2)/2$ resulting in the following expression,

$$\jmath = \pi\rho x^3 \int_0^1 d\mu(1-\mu^2)\int_0^\infty \frac{du}{u^2}\left[1 - J_0(u)\right] = \frac{2\pi}{3}x^3\rho = 0.5\frac{X}{n}\rho \,. \tag{A.9}$$

Hence, by substituting (A.9) in (A.4) we obtain

$$\frac{dP}{dj^2} = \frac{1}{(2\pi)^2}\int \exp\left(\mathrm{i}\rho\cdot\mathbf{j} - \mathrm{j_X}\rho\right)\mathrm{d}\rho^2 \,, \tag{A.10}$$

where $j_X \equiv 0.5X$. Once the probability distribution in two dimensions has been determined, the probability of distribution can be obtained using the zero-order Bessel function as

$$\frac{dP}{dj} = 2\pi j\frac{dP}{d^2j} = \frac{j}{2\pi}\int \exp\left(\mathrm{i}\rho\cdot\mathbf{j} - \mathrm{j_X}\rho\right)\mathrm{d}\rho^2 = \mathrm{j}\int \rho\mathrm{J_0}(\rho\mathrm{j})\mathrm{e}^{-\mathrm{j_X}\rho}\mathrm{d}\rho = \frac{\mathrm{jj_X}}{(\mathrm{j}^2 + \mathrm{j_X^2})^{3/2}} \,. \tag{A.11}$$

The result that we have obtained corresponds to the equation (3.29).

A.1.1. Generalisation of the reduced angular momentum for an extended mass function.

In this subsection, we will generalise the calculations of the probability distribution function of the reduced angular momentum for an extended mass function. For this reason, we have to consider the contribution to the total reduced angular momentum of all PBHs of all possible masses. This reduced angular momentum is given by

$$\mathbf{j} = 3\sum_{l=1}^{P}\sum_{q=1}^{N_l}\frac{M_l}{M_t}\frac{x^3}{y_{l,q}^5}(\hat{x}\cdot\hat{y_{l,q}})(\hat{x}\times\hat{y}_{l,q})\,, \tag{A.12}$$

where $y_{l,q}$ is the comoving separation between the binary and the q-th PBH with mass M_l, N_l are all PBHs with mass M_l and P is the number of possible masses. Hence, we have to rewrite the (A.4) as

$$\frac{dP}{dj^2} = \lim_{V\to\infty}\frac{1}{(2\pi)^2}\int \exp\left(\mathrm{i}\rho\cdot\mathbf{j}\right)\mathrm{A_{N_l}}(\rho)\mathrm{d}\rho^2\,, \tag{A.13}$$

where

$$\begin{aligned} A_{N_l} &= \prod_{l=1}^{P}\prod_{q=1}^{N_l}\left[\int_V \exp\left(-3\mathrm{i}\sum_{\mathrm{n}=1}^{\mathrm{P}}\sum_{\mathrm{m}=1}^{\mathrm{N_n}}\frac{\mathrm{M_n}}{\mathrm{M_t}}\frac{\mathrm{x}^3}{\mathrm{y}_{\mathrm{n,m}}^5}\mathrm{y}_{\mathrm{n,m}\parallel}\rho\cdot\mathbf{y}_{\mathbf{n},\mathbf{m}\perp}\right)\frac{\mathrm{dy_{l,q}^3}}{\mathrm{V}}\right] \\ &= \prod_{l=1}^{P}\left[\int_V \exp\left(-3\mathrm{i}\frac{\mathrm{M_l}}{\mathrm{M_t}}\frac{\mathrm{x}^3}{\mathrm{y}^5}\mathrm{y}_{\parallel}\rho\cdot\mathbf{y}_{\perp}\right)\frac{\mathrm{dy}^3}{\mathrm{V}}\right]^{N_l} \\ &= \prod_{l=1}^{P}\left\{1-\frac{1}{V}\int_V\left[1-\exp\left(-2(1.5)\mathrm{i}\frac{\mathrm{M_l}}{\mathrm{M_t}}\frac{\mathrm{x}^3}{\mathrm{y}^5}\mathrm{y}_{\parallel}\rho\cdot\mathbf{y}_{\perp}\right)\right]\frac{dy^3}{V}\right\}^{n(M_l)V}\,. \end{aligned} \tag{A.14}$$

For simplicity, we will use the following variable change

$$\begin{aligned} I_l &\equiv \left\{1-\frac{1}{V}\int_V\left[1-\exp\left(-2(1.5)\mathrm{i}\frac{\mathrm{x}^3}{\mathrm{y}^5}\mathrm{y}_{\parallel}\,\rho\cdot\mathbf{y}_{\perp}\right)\right]\frac{dy^3}{V}\right\} \\ \jmath_l &\equiv \int_V\left[1-\exp\left(-2(1.5)\mathrm{i}\frac{\mathrm{x}^3}{\mathrm{y}^5}\mathrm{y}_{\parallel}\,\rho\cdot\mathbf{y}_{\perp}\right)\right]\frac{dy^3}{V}\,. \end{aligned} \tag{A.15}$$

So (A.14) becomes

$$\lim_{V\to\infty}A_{N_l} = \lim_{V\to\infty}\prod_{l=1}^{P}I_l = \prod_{l=1}^{P}e^{-\jmath_l n(M_l)}\,. \tag{A.16}$$

This problem is similar to the previous one except for a factor $2M_l/M_t$ in the exponential, and the productory. Therefore, the result obtained in (A.9) will also be a solution to this problem. If we add these factor, the solution of (A.9) is now given by

$$\jmath_l = (2\frac{M_l}{M_t})(\frac{2\pi}{3}x^3\rho) = \frac{4\pi}{3}\frac{M_l}{M_t}x^3\rho\,. \tag{A.17}$$

By substituting this value in the (A.16) equation, we obtain

$$\lim_{V\to\infty} A_{N_l} = \prod_{l=1}^{P} \exp\left(-\frac{4\pi}{3}\frac{\mathrm{M_l}}{\mathrm{M_t}}\mathrm{x}^3\rho\,\mathrm{n(M_l)}\right) = \exp\left(-\frac{4\pi}{3}\sum_{\mathrm{l=1}}^{\mathrm{P}}\frac{\mathrm{M_l n(M_l)}}{\mathrm{M_t}}\mathrm{x}^3\rho\right) . \tag{A.18}$$

It is now easy to see that the summation corresponds to the total mass density of all PBH, i.e. $\rho_{\mathrm{PBH}} = f\rho_{eq}$. Thus, the characteristic value of the reduced angular momentum is given by

$$\lim_{V\to\infty} A_{N_l} = \exp\left(-\frac{4\pi}{3}\frac{\mathrm{f}\rho_{\mathrm{eq}}}{\mathrm{M_t}}\mathrm{x}^3\rho\right) = \exp\left(\,\mathrm{j_X}\rho\,\right) \tag{A.19}$$

$$j_X = \frac{4\pi}{3}\frac{f\rho_{eq}}{M_t}x^3 = 0.5X\,, \tag{A.20}$$

and the reduced angular momentum probability distribution is the same as (A.11).

A.1.2. Reduced angular momentum by other PBHs in a clustered spatial distribution

Finally, we will see how the reduced angular momentum is affected by the clustering effect, considering our approximation done in 3.1.2.2. This subsection is based on the results that we have obtained in the previous subsection for an extended mass function.

Let us start by rewriting the equation (A.14) taking into account that now $N = n\zeta V$,

$$A_{N_{lc}} = \prod_{l=1}^{P}\left\{1 - \frac{1}{V\zeta}\int_V\left[1-\exp\left(-2(1.5)\mathrm{i}\frac{\mathrm{M_l}}{\mathrm{M_t}}\frac{\mathrm{x}^3}{\mathrm{y}^5}\mathrm{y}_{\parallel}\rho\cdot\mathbf{y}_{\perp}\right)\right]\frac{dy^3}{V\zeta}\right\}^{n(M_l)V\zeta} = (1-\jmath_l/V\zeta)^{nV\zeta}\,, \tag{A.21}$$

where $\jmath_l$ is the same as (A.15).

Since the clustering parameter has considered as a finite constant, we will consider that the (A.7) is fulfilled. Thus, the (A.16) equation can be rewritten as

$$\lim_{V\to\infty} A_{N_{lc}} = \lim_{V\to\infty}\prod_{l=1}^{P} I_l = \prod_{l=1}^{P} e^{-\jmath_l n(M_l)\zeta}\,. \tag{A.22}$$

Since $\jmath_l$ has the same value, we will solve this problem in a similar way as in the previous sections. However, It is noteworthy that there is a change in the equation (A.18), where in this case we have the expression

$$\begin{aligned}\lim_{V\to\infty} A_{N_l} = \prod_{l=1}^{P}\exp\left(-\frac{4\pi}{3}\frac{\mathrm{M_l}}{\mathrm{M_t}}\mathrm{x}^3\rho\,\mathrm{n(M_l)}\zeta\right) &= \exp\left(-\frac{4\pi}{3}\sum_{\mathrm{l=1}}^{\mathrm{P}}\frac{\mathrm{M_l n(M_l)}}{\mathrm{M_t}}\mathrm{x}^3\rho\zeta\right)\\ &= \exp\left(-\frac{4\pi}{3}\frac{\mathrm{f}\rho_{\mathrm{eq}}}{\mathrm{M_t}}\mathrm{x}^3\rho\zeta\right) = \exp\left(\,\mathrm{j_X}\rho\,\right)\,,\end{aligned} \tag{A.23}$$

where using the result obtained in (3.4), we get the same expression of j_x as in the above cases.

Bibliography

[1] N. Aghanim, Y. Akrami, M. Ashdown, J. Aumont, C. Baccigalupi, M. Ballardini, A. J. Banday, R. B. Barreiro, N. Bartolo, and et al. "Planck 2018 results". In: *Astronomy Astrophysics* 641 (2020), A6. ISSN: 1432-0746. DOI: 10.1051/0004-6361/201833910. URL: http://dx.doi.org/10.1051/0004-6361/201833910.

[2] Juan García-Bellido. "Primordial black holes and the origin of the matter–antimatter asymmetry". In: *Phil. Trans. Roy. Soc. Lond. A* 377.2161 (2019). Ed. by John Dainton, p. 20190091. DOI: 10.1098/rsta.2019.0091.

[3] Masahiro Morikawa. "Galaxy Formation from the Primordial Black Holes". In: *EPJ Web of Conferences* 164 (Jan. 2017), p. 01011. DOI: 10.1051/epjconf/201716401011.

[4] Anne M Green and Bradley J Kavanagh. "Primordial black holes as a dark matter candidate". In: *Journal of Physics G: Nuclear and Particle Physics* 48.4 (2021), p. 043001. ISSN: 1361-6471. DOI: 10.1088/1361-6471/abc534. URL: http://dx.doi.org/10.1088/1361-6471/abc534.

[5] B. J. Carr, Kazunori Kohri, Yuuiti Sendouda, and Jun'ichi Yokoyama. "New cosmological constraints on primordial black holes". In: *Physical Review D* 81.10 (2010). ISSN: 1550-2368. DOI: 10.1103/physrevd.81.104019. URL: http://dx.doi.org/10.1103/PhysRevD.81.104019.

[6] Roberta Calabrese, Damiano F. G. Fiorillo, Gennaro Miele, Stefano Morisi, and Antonio Palazzo. *Primordial Black Hole Dark Matter evaporating on the Neutrino Floor*. 2021. arXiv: 2106.02492 [hep-ph].

[7] Hiroko Niikura, Masahiro Takada, Naoki Yasuda, Robert H. Lupton, Takahiro Sumi, Surhud More, Toshiki Kurita, Sunao Sugiyama, Anupreeta More, Masamune Oguri, and et al. "Microlensing constraints on primordial black holes with Subaru/HSC Andromeda observations". In: *Nature Astronomy* 3.6 (2019), 524–534. ISSN: 2397-3366. DOI: 10.1038/s41550-019-0723-1. URL: http://dx.doi.org/10.1038/s41550-019-0723-1.

[8] M. R. S. Hawkins. "Gravitational microlensing, quasar variability and missing matter". In: *Nature* 366.6452 (1993), pp. 242–245. DOI: 10.1038/366242a0.

[9] Miguel Zumalacárregui and Uroš Seljak. "Limits on Stellar-Mass Compact Objects as Dark Matter from Gravitational Lensing of Type Ia Supernovae". In: *Physical Review Letters* 121.14 (2018). ISSN: 1079-7114. DOI: 10.1103/physrevlett.121.141101. URL: http://dx.doi.org/10.1103/PhysRevLett.121.141101.

[10] Katherine J. Mack, Jeremiah P. Ostriker, and Massimo Ricotti. "Growth of Structure Seeded by Primordial Black Holes". In: *The Astrophysical Journal* 665.2 (2007), 1277–1287. ISSN: 1538-4357. DOI: 10.1086/518998. URL: http://dx.doi.org/10.1086/518998.

[11] A. Ewall-Wice, T.-C. Chang, J. Lazio, O. Doré, M. Seiffert, and R. A. Monsalve. "Modeling the Radio Background from the First Black Holes at Cosmic Dawn: Implications for the 21 cm Absorption Amplitude". In: *The Astrophysical Journal* 868.1 (2018), p. 63. ISSN: 1538-4357. DOI: 10.3847/1538-4357/aae51d. URL: http://dx.doi.org/10.3847/1538-4357/aae51d.

[12] Kazunori Kohri, Tomohiro Nakama, and Teruaki Suyama. "Testing scenarios of primordial black holes being the seeds of supermassive black holes by ultracompact minihalos and CMBdistortions". In: *Physical Review D* 90.8 (2014). ISSN: 1550-2368. DOI: 10.1103/physrevd.90.083514. URL: http://dx.doi.org/10.1103/PhysRevD.90.083514.

[13] Fabio Capela, Maxim Pshirkov, and Peter Tinyakov. "Constraints on primordial black holes as dark matter candidates from capture by neutron stars". In: *Physical Review D* 87.12 (2013). ISSN: 1550-2368. DOI: 10.1103/physrevd.87.123524. URL: http://dx.doi.org/10.1103/PhysRevD.87.123524.

[14] Miguel A. Monroy-Rodríguez and Christine Allen. "THE END OF THE MACHO ERA, REVISITED: NEW LIMITS ON MACHO MASSES FROM HALO WIDE BINARIES". In: *The Astrophysical Journal* 790.2 (2014), p. 159. ISSN: 1538-4357. DOI: 10.1088/0004-637x/790/2/159. URL: http://dx.doi.org/10.1088/0004-637X/790/2/159.

[15] B.P. Abbott, R. Abbott, T.D. Abbott, F. Acernese, K. Ackley, C. Adams, T. Adams, P. Addesso, R.X. Adhikari, V.B. Adya, and et al. "GW170104: Observation of a 50-Solar-Mass Binary Black Hole Coalescence at Redshift 0.2". In: *Physical Review Letters* 118.22 (2017). ISSN: 1079-7114. DOI: 10.1103/physrevlett.118.221101. URL: http://dx.doi.org/10.1103/PhysRevLett.118.221101.

[16] Sebastien Clesse, Juan García-Bellido, and Stefano Orani. *Detecting the Stochastic Gravitational Wave Background from Primordial Black Hole Formation*. 2018. arXiv: 1812.11011 [astro-ph.CO].

[17] B. J. Carr. "Some cosmological consequences of primordial black-hole evaporations." In: 206 (May 1976), pp. 8–25. DOI: 10.1086/154351.

[18] B. J. Carr and S. W. Hawking. "Black Holes in the Early Universe". In: *Monthly Notices of the Royal Astronomical Society* 168.2 (Aug. 1974), pp. 399–415. ISSN: 0035-8711. DOI: 10.1093/mnras/168.2.399. eprint: https://academic.oup.com/mnras/article-pdf/168/2/399/8079885/mnras168-0399.pdf. URL: https://doi.org/10.1093/mnras/168.2.399.

[19] J. C. Niemeyer and K. Jedamzik. "Dynamics of primordial black hole formation". In: *Physical Review D* 59.12 (1999). ISSN: 1089-4918. DOI: 10.1103/physrevd.59.124013. URL: http://dx.doi.org/10.1103/PhysRevD.59.124013.

[20] Juan García-Bellido, José Francisco Nuño Siles, and Ester Ruiz Morales. "Bayesian analysis of the spin distribution of LIGO/Virgo black holes". In: *Physics of the Dark Universe* 31 (2021), p. 100791. ISSN: 2212-6864. DOI: 10.1016/j.dark.2021.100791. URL: http://dx.doi.org/10.1016/j.dark.2021.100791.

[21] Yacine Ali-Haïmoud, Ely D. Kovetz, and Marc Kamionkowski. "Merger rate of primordial black-hole binaries". In: *Physical Review D* 96.12 (2017). ISSN: 2470-0029. DOI: 10.1103/physrevd.96.123523. URL: http://dx.doi.org/10.1103/PhysRevD.96.123523.

[22] P C Peters. "GRAVITATIONAL RADIATION AND THE MOTION OF TWO POINT MASSES". In: *Physical Review (U.S.) Superseded in part by Phys. Rev. A, Phys. Rev. B: Solid State, Phys. Rev. C, and Phys. Rev. D* (). DOI: 10.1103/PhysRev.136.B1224. URL: https://www.osti.gov/biblio/4688457.

[23] P. C. Peters and J. Mathews. "Gravitational Radiation from Point Masses in a Keplerian Orbit". In: *Phys. Rev.* 131 (1 1963), pp. 435–440. DOI: 10.1103/PhysRev.131.435. URL: https://link.aps.org/doi/10.1103/PhysRev.131.435.

[24] M. P. Hobson, G. P. Efstathiou, and A. N. Lasenby. *General Relativity: An Introduction for Physicists*. Cambridge University Press, 2006. DOI: 10.1017/CBO9780511790904.

[25] LIGO and Virgo collaboration. *Gravitational Wave Open Science Center*. URL: https://www.gw-openscience.org/tutorial06/ (visited on 06/24/2021).

[26] Zu-Cheng Chen and Qing-Guo Huang. "Merger Rate Distribution of Primordial Black Hole Binaries". In: *The Astrophysical Journal* 864.1 (2018), p. 61. ISSN: 1538-4357. DOI: 10.3847/1538-4357/aad6e2. URL: http://dx.doi.org/10.3847/1538-4357/aad6e2.

[27] Martti Raidal, Ville Vaskonen, and Hardi Veermäe. "Gravitational waves from primordial black hole mergers". In: *Journal of Cosmology and Astroparticle Physics* 2017.09 (2017), 037–037. ISSN: 1475-7516. DOI: 10.1088/1475-7516/2017/09/037. URL: http://dx.doi.org/10.1088/1475-7516/2017/09/037.

[28] The LIGO Scientific Collaboration et al. *Population Properties of Compact Objects from the Second LIGO-Virgo Gravitational-Wave Transient Catalog*. 2021. arXiv: 2010.14533 [astro-ph.HE].

[29] B.J. Carr, Kazunori Kohri, Yuuiti Sendouda, and Jun'ichi Yokoyama. "Constraints on primordial black holes from the Galactic gamma-ray background". In: *Physical Review D* 94.4 (2016). ISSN: 2470-0029. DOI: 10.1103/physrevd.94.044029. URL: http://dx.doi.org/10.1103/PhysRevD.94.044029.

[30] Bernard Carr, Martti Raidal, Tommi Tenkanen, Ville Vaskonen, and Hardi Veermäe. "Primordial black hole constraints for extended mass functions". In: *Physical Review D* 96.2 (2017). ISSN: 2470-0029. DOI: 10.1103/physrevd.96.023514. URL: http://dx.doi.org/10.1103/PhysRevD.96.023514.

[31] Guillermo Ballesteros, Pasquale D. Serpico, and Marco Taoso. "On the merger rate of primordial black holes: effects of nearest neighbours distribution and clustering". In: *Journal of Cosmology and Astroparticle Physics* 2018.10 (2018), 043–043. ISSN: 1475-7516. DOI: 10.1088/1475-7516/2018/10/043. URL: http://dx.doi.org/10.1088/1475-7516/2018/10/043.

[32] Yu N Eroshenko. "Gravitational waves from primordial black holes collisions in binary systems". In: *Journal of Physics: Conference Series* 1051 (2018), p. 012010. ISSN: 1742-6596. DOI: 10.1088/1742-6596/1051/1/012010. URL: http://dx.doi.org/10.1088/1742-6596/1051/1/012010.

[33] Ville Vaskonen and Hardi Veermäe. "Lower bound on the primordial black hole merger rate". In: *Physical Review D* 101.4 (2020). ISSN: 2470-0029. DOI: 10.1103/physrevd.101.043015. URL: http://dx.doi.org/10.1103/PhysRevD.101.043015.

[34] Alexander H. Nitz and Yi-Fan Wang. *Search for gravitational waves from the coalescence of sub-solar mass and eccentric compact binaries*. 2021. arXiv: 2102.00868 [astro-ph.HE].

[35] Alexander H. Nitz and Yi-Fan Wang. *Search for gravitational waves from the coalescence of sub-solar mass binaries in the first half of Advanced LIGO and Virgo's third observing run*. 2021. arXiv: 2106.08979 [astro-ph.HE].

[36] B.P. Abbott, R. Abbott, T.D. Abbott, S. Abraham, F. Acernese, K. Ackley, A. Adams, C. Adams, R.X. Adhikari, V.B. Adya, and et al. "Search for intermediate mass black hole binaries in the first and second observing runs of the Advanced LIGO and Virgo network". In: *Physical Review D* 100.6 (2019). ISSN: 2470-0029. DOI: 10.1103/physrevd.100.064064. URL: http://dx.doi.org/10.1103/PhysRevD.100.064064.

[37] Gert Hütsi, Martti Raidal, Ville Vaskonen, and Hardi Veermäe. "Two populations of LIGO-Virgo black holes". In: *Journal of Cosmology and Astroparticle Physics* 2021.03 (2021), p. 068. ISSN: 1475-7516. DOI: 10.1088/1475-7516/2021/03/068. URL: http://dx.doi.org/10.1088/1475-7516/2021/03/068.

[38] José Luis Bernal, Nicola Bellomo, Alvise Raccanelli, and Licia Verde. "Cosmological implications of primordial black holes". In: *Journal of Cosmology and Astroparticle Physics* 2017.10 (2017), 052–052. ISSN: 1475-7516. DOI: 10.1088/1475-7516/2017/10/052. URL: http://dx.doi.org/10.1088/1475-7516/2017/10/052.

[39] Simeon Bird, Ilias Cholis, Julian B. Muñoz, Yacine Ali-Haïmoud, Marc Kamionkowski, Ely D. Kovetz, Alvise Raccanelli, and Adam G. Riess. "Did LIGO Detect Dark Matter?" In: *Physical Review Letters* 116.20 (2016). ISSN: 1079-7114. DOI: 10.1103/physrevlett.116.201301. URL: http://dx.doi.org/10.1103/PhysRevLett.116.201301.

[40] Bradley J. Kavanagh, Daniele Gaggero, and Gianfranco Bertone. "Merger rate of a subdominant population of primordial black holes". In: *Physical Review D* 98.2 (2018). ISSN: 2470-0029. DOI: 10.1103/physrevd.98.023536. URL: http://dx.doi.org/10.1103/PhysRevD.98.023536.

[41] S. Chandrasekhar. “Stochastic Problems in Physics and Astronomy”. In: *Rev. Mod. Phys.* 15 (1 1943), pp. 1–89. DOI: 10.1103/RevModPhys.15.1. URL: https://link.aps.org/doi/10.1103/RevModPhys.15.1.